OPEN

MicroRNA-181b Controls Atherosclerosis and Aneurysms Through Regulation of TIMP-3 and Elastin

Karina Di Gregoli, Nur Najmi Mohamad Anuar, Rosaria Bianco, Stephen J. White, Andrew C. Newby, Sarah J. George, Jason L. Johnson

Rationale: **Atherosclerosis and aneurysms are leading causes of mortality worldwide. MicroRNAs (miRs) are key determinants of gene and protein expression, and atypical miR expression has been associated with many cardiovascular diseases; although their contributory role to atherosclerotic plaque and abdominal aortic aneurysm stability are poorly understood.**

Objective: **To investigate whether miR-181b regulates tissue inhibitor of metalloproteinase-3 expression and affects atherosclerosis and aneurysms.**

Methods and Results: **Here, we demonstrate that miR-181b was overexpressed in symptomatic human atherosclerotic plaques and abdominal aortic aneurysms and correlated with decreased expression of predicted miR-181b targets, tissue inhibitor of metalloproteinase-3, and elastin. Using the well-characterized mouse atherosclerosis models of *Apoe*$^{-/-}$ and *Ldlr*$^{-/-}$, we observed that in vivo administration of locked nucleic acid anti-miR-181b retarded both the development and the progression of atherosclerotic plaques. Systemic delivery of anti-miR-181b in angiotensin II–infused *Apoe*$^{-/-}$ and *Ldlr*$^{-/-}$ mice attenuated aneurysm formation and progression within the ascending, thoracic, and abdominal aorta. Moreover, miR-181b inhibition greatly increased elastin and collagen expression, promoting a fibrotic response and subsequent stabilization of existing plaques and aneurysms. We determined that miR-181b negatively regulates macrophage tissue inhibitor of metalloproteinase-3 expression and vascular smooth muscle cell elastin production, both important factors in maintaining atherosclerotic plaque and aneurysm stability. Validation studies in *Timp3*$^{-/-}$ mice confirmed that the beneficial effects afforded by miR-181b inhibition are largely tissue inhibitor of metalloproteinase-3 dependent, while also revealing an additional protective effect through elevating elastin synthesis.**

Conclusions: **Our findings suggest that the management of miR-181b and its target genes provides therapeutic potential for limiting the progression of atherosclerosis and aneurysms and protecting them from rupture. (*Circ Res*. 2017;120:49-65. DOI: 10.1161/CIRCRESAHA.116.309321.)**

Key Words: aortic aneurysm, abdominal ■ atherosclerosis ■ macrophages ■ microRNAs ■ tissue inhibitor of metalloproteinase-3

Atherosclerosis and aneurysms are the leading causes of cardiovascular disease, the major source of mortality and morbidity worldwide.[1] Unstable atherosclerotic plaques are characterized by a relative preponderance of inflammatory cells and heightened proteolytic activity.[2,3] Clinically relevant abdominal aortic aneurysms (AAAs) are also associated with inflammation and matrix degradation.[4] Subsets of proinflammatory macrophages are considered central to the pathogenesis of the above inflammatory cardiovascular diseases, in part, through augmented release of matrix-degrading proteases and by decreased expression of their inhibitors. However, other macrophage subsets may play beneficial roles, for example, by facilitating smooth muscle cell recruitment, regulating neovascularization, and promoting extracellular matrix (ECM) formation/deposition.[5] Similarly, matrix metalloproteinases (MMPs), a group of proteases produced by macrophages and abundant in pathological cardiovascular tissues,[6] may also play a dual role. MMP knockout mice and other transgenic models show clear effects of individual MMPs on vascular repair and fibrous cap formation on the one hand or ECM destruction and hence destabilization of atherosclerotic lesions and aneurysm rupture on the other. These opposing effects of different MMPs probably underlie the disappointing results achieved

Editorial, see p 5
In This Issue, see p 2

Original received June 14, 2016; revision received October 13, 2016; accepted October 18, 2016. In September 2016, the average time from submission to first decision for all original research papers submitted to *Circulation Research* was 12.73 days.

From the Laboratory of Cardiovascular Pathology, School of Clinical Sciences, University of Bristol, England.

The online-only Data Supplement is available with this article at http://circres.ahajournals.org/lookup/suppl/doi:10.1161/CIRCRESAHA.116.309321/-/DC1.

Correspondence to Jason L. Johnson, PhD, Laboratory of Cardiovascular Pathology, School of Clinical Sciences, Faculty of Health Sciences, University of Bristol, Level 7, Bristol Royal Infirmary, Bristol BS2 8HW, England. E-mail jason.l.johnson@bristol.ac.uk

Circulation Research **is available at http://circres.ahajournals.org** **DOI: 10.1161/CIRCRESAHA.116.309321**

Nonstandard Abbreviations and Acronyms	
AAA	abdominal aortic aneurysm
Apoe	apolipoprotein E
ECM	extracellular matrix
GM-CSF	granulocyte/macrophage colony-stimulating factor
Ldlr	low-density lipoprotein receptor
M-CSF	macrophage colony-stimulating factor
miR	microRNA
MMP	matrix metalloproteinase
TIMP	tissue inhibitor of metalloproteinase
VSMC	vascular smooth muscle cell

with broad-spectrum MMP inhibitors in these pathologies.[7] However, altering levels of tissue inhibitors of metalloproteinases (TIMPs) have revealed more consistent protective effects against atherosclerosis and aneurysm formation.[7] Hence, understanding and manipulating the factors that regulate TIMP production in macrophages may provide new therapeutic avenues.

Previous studies from our laboratory identified a distinct subpopulation of macrophages with reduced TIMP-3 expression and a concomitant increase in MMP-14 protein level and activity and associated proteolysis.[8] TIMP-3–negative macrophages are more invasive, more susceptible to apoptosis, and more proliferative compared with the TIMP-3–positive macrophage subpopulation[8] and are more abundant in unstable than stable plaques.[9] Further analysis revealed that granulocyte macrophage colony-stimulating factor (GM-CSF) increased MMP-14 protein but not mRNA level by decreasing expression of microRNA (miR)-24, resulting in increased MMP-14–dependent proteolytic activity.[10] GM-CSF consequently promoted a more invasive and proapoptotic macrophage phenotype, which was associated with unstable atherosclerotic plaques.[10] Some evidence suggested that macrophage TIMP-3 expression may also be subjected to post-transcriptional regulation.[8,9] MiRs are a group of noncoding RNAs able to finely regulate the protein expression of their targets through degradation of the mRNA or inhibition of protein translation. MiRs control several processes known to be involved with the initiation and progression of numerous cardiovascular diseases, such as atherosclerosis[11] and AAAs.[12] In particular, miR-181b is a highly conserved miR able to directly target TIMP-3 mRNA and repress TIMP-3 protein expression in hepatocarcinoma cells.[13] In addition, miR-181b is downregulated during macrophage colony-stimulating factor (M-CSF) maturation of macrophages,[10] whereas TIMP-3 protein and mRNA expression is enhanced.[14] TIMP-3 has been identified in atherosclerotic plaque macrophages between the necrotic/lipid-rich core and the protective fibrous cap.[14] Consequently, TIMP-3 may play a protective role against plaque rupture through suppressing local proteolysis. TIMP-3 mRNA levels are also increased in patients with ascending aortic aneurysms, whereas other TIMPs are not altered.[15] Similarly, a significant association between polymorphisms of TIMP-3, but not TIMP-1 or TIMP-2, exists in patients with AAA and a positive family history of AAA.[16] Also, aorta wall TIMP-3 expression is reduced in Marfan syndrome patients who experience an increased rate of aortic rupture.[17]

Hence, in the current study, we investigated whether miR-181b regulates TIMP-3 protein expression in atherosclerosis and AAA and whether miR-181b inhibition can ameliorate plaque and aneurysm progression. Consequently, we demonstrate for the first time that miR-181b inhibition promotes a stable plaque phenotype by restoring TIMP-3 expression in macrophages, which stabilizes AAAs by promoting collagen accumulation. Inhibition of miR-181b also directly enhances elastin deposition. This dual beneficial role of miR-181b inhibition provides substantial evidence for this approach as a therapeutic for atherosclerosis-related cardiovascular diseases, including aneurysms.

Methods

Methods are available in the Online Data Supplement.

Results

MiR-181b Regulates Macrophage TIMP-3 Expression and Associates With Cardiovascular Disease Progression in Humans

We first measured TIMP-3 levels in macrophages, differentiated with M-CSF or GM-CSF, respectively.[18] Although no difference in *TIMP3* mRNA expression was detected (Figure 1A), protein levels were markedly reduced in GM-CSF–differentiated macrophages (Figure 1B). Accordingly, the level of miR-181b was significantly increased after GM-CSF macrophage differentiation compared with M-CSF macrophages (Figure 1C), implying that it could be responsible for the fall in TIMP-3 protein. To confirm this, we deployed a loss of function strategy in GM-CSF macrophages, revealing that miR-181b inhibition restored TIMP-3 protein expression to comparable levels found in M-CSF macrophages (Figure 1D), whereas the mRNA level was significantly reduced (Figure 1E), implying restored *TIMP3* translation. Hence, our findings confirm TIMP-3 as an miR-181b target[13] and demonstrate that miR-181b serves as an important inhibitor of macrophage TIMP-3 protein expression, which is divergently regulated by colony-stimulating factors. Moreover, these changes are independent of potential regulation by MMP-14 expression/activity, which we have previously shown to be upregulated in macrophages on GM-CSF stimulation[10] or through regulation of MMP-14 expression by miR-181b or TIMP-3 (Online Figure I).

To validate our findings in human cardiovascular pathologies, we investigated the expression of miR-181b and its putative target TIMP-3 in human coronary atherosclerotic plaques and AAAs. We observed a decreased proportion of TIMP-3–positive macrophages ($CD68^{+ve}$ cells) in human coronary artery atherosclerotic plaques characterized as unstable compared with stable lesions (by 67%; $P<0.01$; Figure 1F), whereas no change in *TIMP3* mRNA expression was detected (Online Figure II). Furthermore, miR-181b expression in atherosclerotic plaques was inversely related to TIMP-3 protein expression because unstable plaques contained higher miR-181b levels (as assessed by quantitative polymerase chain reaction) than stable plaques (28-fold; $P<0.05$; Figure 1G). Moreover, confirmatory in situ hybridization indicated that the proportion of macrophages expressing miR-181b was

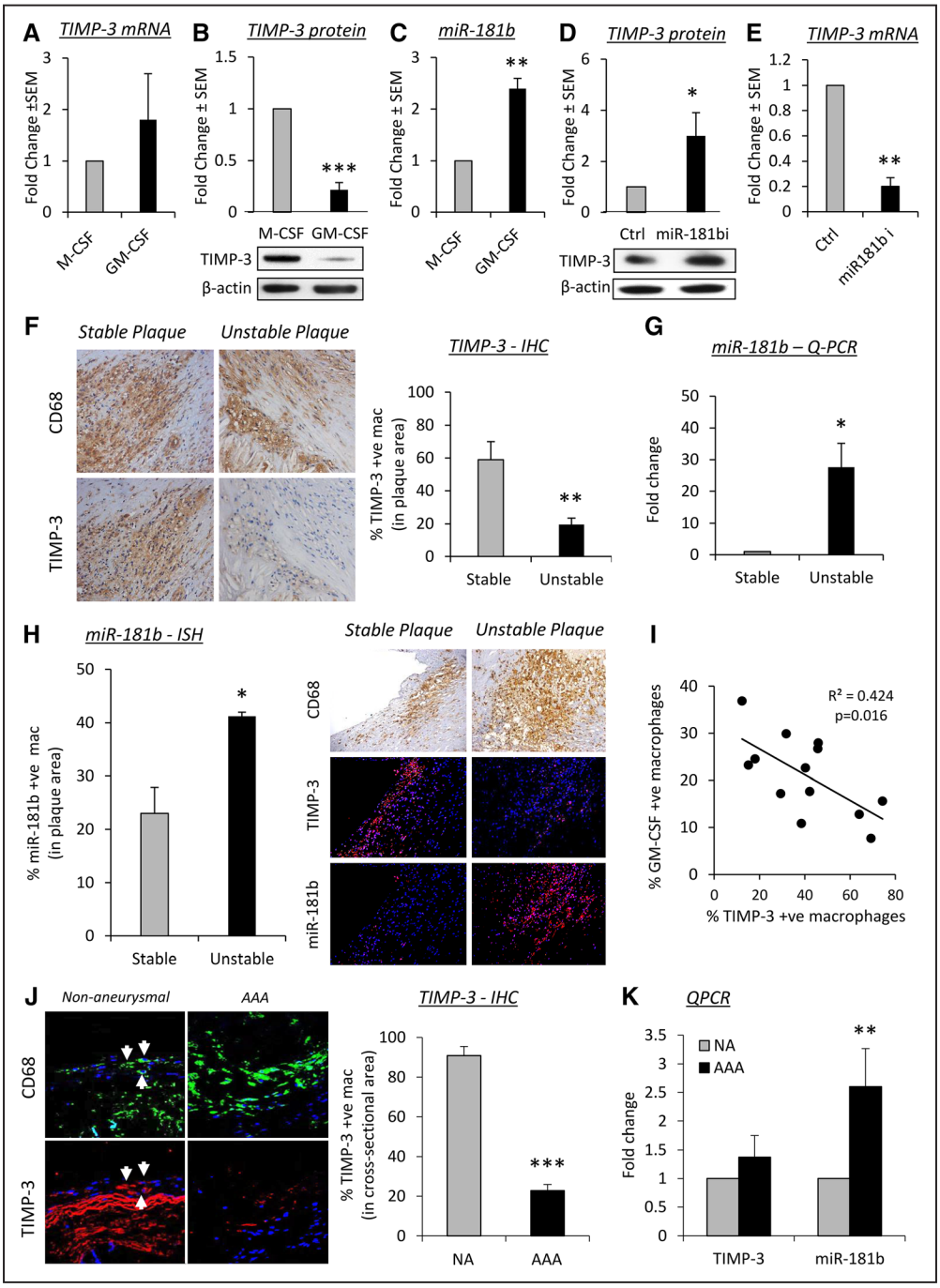

Figure 1. MicroRNA (miR)-181b regulates macrophage tissue inhibitor of metalloproteinase (TIMP)-3 expression and associates with cardiovascular disease progression in humans. **A**, Quantitative polymerase chain reaction (QPCR) and (**B**) Western blot of *TIMP3* mRNA and protein expression, respectively, in human macrophages differentiated in the presence of macrophage colony-stimulating factor (M-CSF) or granulocyte/macrophage colony-stimulating factor (GM-CSF), n=6/group, ***P<0.001, 2-tailed Student t test. **C**, QPCR of miR-181b in human macrophages differentiated in the presence of M-CSF or GM-CSF, n=6/group, **P<0.01, 2-tailed Student t test. **D**, Western blot and (**E**) QPCR of *TIMP3* in 7-day GM-CSF–differentiated macrophages after addition of an miR-181b inhibitor (miR-181bi) or a scrambled control (Ctrl), n=4/group, *P<0.05 and **P<0.05, 2-tailed Student t test. **F**, Representative images of CD68 (macrophages) and TIMP-3 protein expression by immunohistochemistry (IHC) and quantification from human stable and unstable coronary atherosclerotic plaques, n=10/group, **P<0.01, 2-tailed Student t test. **G**, QPCR of miR-181b expression from stable and unstable coronary atherosclerotic plaques, n=10/group, *P<0.05, 2-tailed Student t test. **H**, Representative images and quantification of TIMP-3 protein expression by IHC and miR-181b by in situ hybridization (ISH) from stable and unstable coronary atherosclerotic plaques, n=10/group, *P<0.05, 2-tailed Student t test. **I**, Correlation of TIMP-3 and GM-CSF–positive macrophages in human coronary artery atherosclerotic plaques, n=16, Spearman correlation test. **J**, Representative images of CD68 (macrophages) and TIMP-3 protein expression by IHC and quantification from control human nonaneurysmal (NA) aorta and abdominal aortic aneurysm (AAA), n=10/group, ***P<0.00315, 2-tailed Student t test. **K**, QPCR of TIMP-3 and miR-181b expression from control human NA aorta and AAA, n=10/group, **P<0.01, 2-tailed Student t test. In all cases, data represent the mean±SEM.

significantly higher in unstable plaques compared with stable plaques ($P<0.05$; Figure 1H and Online Figure III) in direct contrast to TIMP-3 protein expression (Figure 1E). We previously showed that unstable human coronary plaques harbor a heightened proportion of GM-CSF than M-CSF–positive macrophage.[10] We now show that the density of intraplaque TIMP-3–positive macrophages negatively correlated with the number of GM-CSF–positive macrophages in advanced plaques ($r^2=0.424$; $P=0.016$; Figure 1I).

Similar findings were apparent in human aortic aneurysm tissues. Whereas the majority of macrophages ($CD68^{+ve}$ cells) in nonaneurysmal aortic tissue were TIMP-3 positive (91%; Figure 1J), only 23% of macrophages within abdominal aortic tissues expressed TIMP-3 (Figure 1J). These differences were independent of alterations in mRNA expression (Figure 1K), but consistent with the significant change in miR-181b levels we observed (Figure 1K). Accordingly, areas of macrophage infiltration in AAA tissues were associated with marked MMP activity (Online Figure IV). Furthermore, using the angiotensin II infusion model of AAA in 8-week-old high-fat–fed apolipoprotein E–deficient (*Apoe*$^{-/-}$) mice, we investigated macrophage TIMP-3 expression within intact and ruptured abdominal aortas. As in human tissues, significantly more TIMP-3–positive macrophages (3-fold; $P=0.00315$) were present in intact abdominal aortic tissues compared with ruptured aneurysmal samples (Online Figure V). Taken together, our results imply that miR-181b is a critical regulator of macrophage TIMP-3 expression during the progression of atherosclerosis and aortic aneurysms.

MiR-181b Inhibition Stabilizes Atherosclerotic Plaques in Hypercholesterolemic *Apoe*$^{-/-}$ Mice

Given the above, we hypothesized that miR-181b inhibition may restore macrophage TIMP-3 expression and prevent the progression of atherosclerosis. Therefore, mice with preexisting atherosclerotic lesions within their brachiocephalic arteries were treated with a locked nucleic acid–modified miR-181b inhibitor or a scrambled miR to serve as a control (n=6–8 per group; see Online Figure VI). Body weights were comparable between scrambled control (29.7±1.1 g) and miR-181b inhibitor-treated mice (30.2±1.3 g), indicating that locked nucleic acid–miR treatment was well tolerated, and no significant effect on lipid profiles was observed (Online Figure VII). Quantitative polymerase chain reaction analysis of atherosclerotic vessels demonstrated reduced miR-181b expression in mice treated with the locked nucleic acid–miR-181b inhibitor controls (Online Figure VIII), inferring that the miR-181b inhibitor had pervaded the plaque/vessel wall. As expected, miR-181b inhibition resulted in a significant increase in intraplaque TIMP-3–positive macrophages (by 90%; $P<0.05$; Figure 2A). As expected, proteolytic activity was abrogated within plaques from miR-181b inhibitor-treated mice when compared with controls (by 70%; $P<0.01$; Figure 2B), as ascertained by in situ zymography, and comparable with the inhibitory effect achieved by addition of exogenous TIMP-3 (Figure 2B). Furthermore, recombinant TIMP-3 displayed no additive inhibitory effect on proteolytic activity in plaques from miR-181b inhibitor-treated animals (Figure 2B), indicating that the miR-181b inhibition-associated increase in TIMP-3 expression was responsible for the diminished proteolytic activity observed in plaques from treated mice. Hence, the TIMP-3–dependent reduction in proteolytic activity afforded through miR-181b inhibition translated into a retardation of plaque progression when compared with control animals, as observed by a reduction in lesion area (by 45%; $P<0.05$; Figure 2C and 2D).

In addition, pathological characteristics associated with a more stable plaque phenotype were increased in treated mice compared with control animals; smooth muscle cell to macrophage ratio (4.9-fold increase; $P<0.01$; Figure 2C and 2E), collagen content (59% increase; $P<0.01$; Figure 2C and 2F), and necrotic/lipid core size (42% decrease; $P<0.05$; Figure 2C and 2G). Moreover, and in line with our previous in vitro data,[8] intraplaque macrophage proliferation rates and apoptotic frequencies were reduced (88% and 68%, respectively; $P<0.01$; Figure 2C, 2H, and 2I) in brachiocephalic plaques from miR-181b inhibitor-treated mice compared with scrambled control animals. Collectively, miR-181b inhibition resulted in alterations in plaque composition that have been previously taken as markers of increased plaque stability. Consistent with this, the lesion compositional changes translated to a decreased plaque vulnerability index[19] in mice receiving miR-181b inhibition compared with scrambled control animals (by 73%; $P<0.01$; Figure 2C and 2J). Finally, miR-181b inhibition significantly augmented elastin content within plaques compared with scrambled control animals (2.6-fold; $P<0.01$; Figure 2C and 2K). Collectively, these results suggest that inhibition of miR-181b dramatically increases macrophage TIMP-3 expression and thus retards plaque progression and promotes a more stable phenotype.

We also subjected 10-week high-fat–fed low-density lipoprotein receptor knockout mice (*Ldlr*$^{-/-}$), which have preexisting atherosclerotic lesions within their brachiocephalic arteries (Online Figure IX) to 4-week treatment with the locked nucleic acid–modified miR-181b inhibitor or a scrambled miR to serve as control animals, while being maintained on a high-fat diet (n=6–8 per group, see Online Figure IV). Similar to *Apoe*$^{-/-}$ mice, we observed a significant suppression in plaque progression as observed by a reduction in lesion area of miR-181b inhibitor-treated mice versus controls (by 67%; $P<0.05$; Online Figure IV), indicating that this effect is not exclusive to the *Apoe*$^{-/-}$ mouse model.

MiR-181b Inhibition Does Not Affect Plaque Progression in the Absence of TIMP-3

To assess whether miR-181b inhibition modulates atherosclerotic plaque progression through TIMP-3, we measured plaque development in *Apoe/Timp3* double knockout (*Timp3*$^{-/-}$/*Apoe*$^{-/-}$) mice and whether miR-181b inhibition retarded the progression of preexisting lesions, as observed in *Apoe* knockout mice. After 12 weeks of high-fat feeding and as expected, *Timp3*$^{-/-}$/*Apoe*$^{-/-}$ mice displayed accelerated atherosclerosis compared with control *Timp3*$^{+/+}$/*Apoe*$^{-/-}$ animals, as assessed by morphometric analyses of lesion area in cross-sections of the aortic root (2.5-fold; $P<0.05$; Figure 3A) and the brachiocephalic artery (5.7-fold; $P<0.05$; Figure 3B). In contrast to *Apoe*$^{-/-}$ mice (Figure 2D), miR-181b inhibition failed to retard plaque progression at either vascular site, in *Timp3*$^{-/-}$/*Apoe*$^{-/-}$

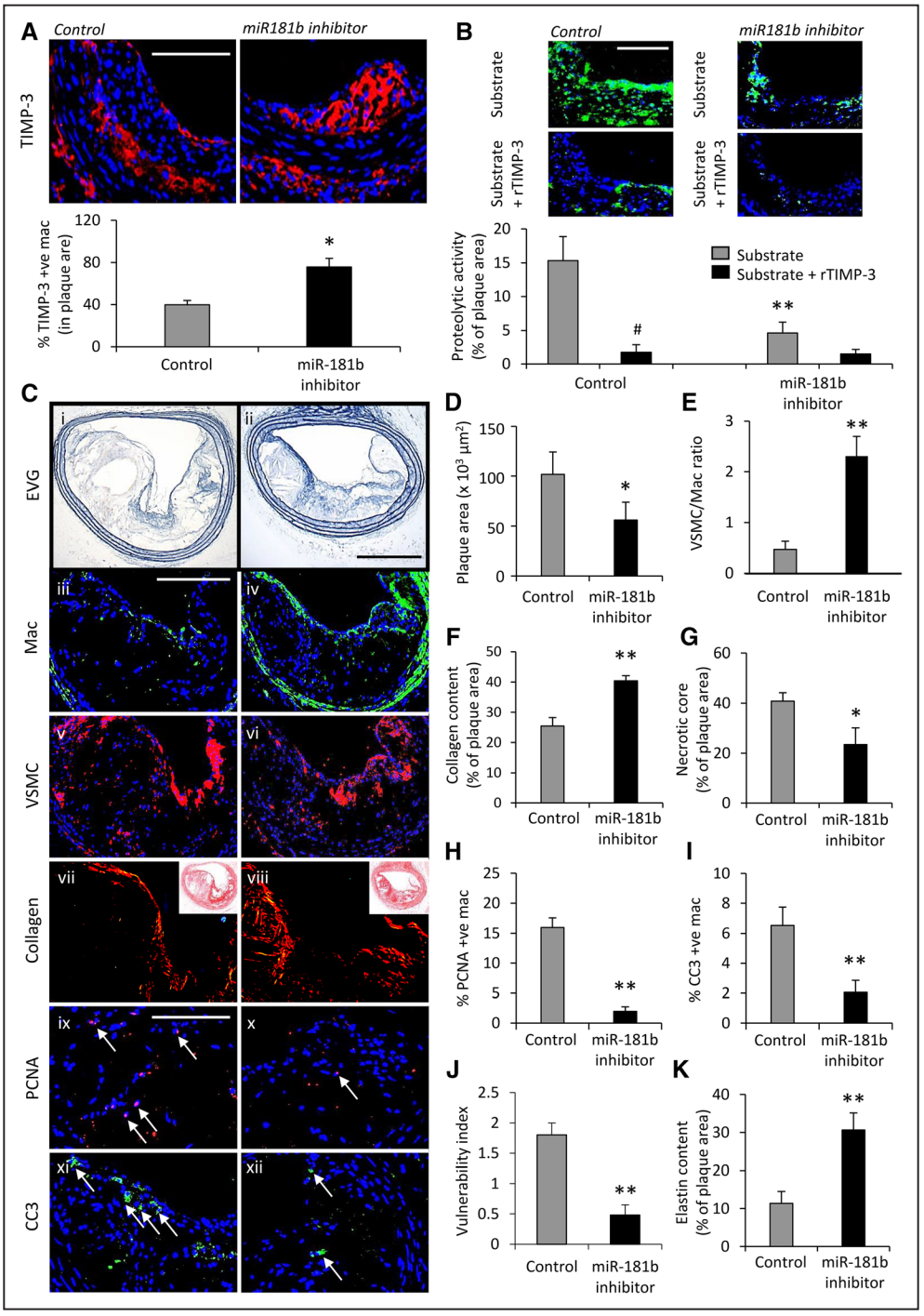

Figure 2. MicroRNA (miR)-181b inhibition stabilizes atherosclerotic plaques in hypercholesterolemic *Apoe*$^{-/-}$ mice. **A**, Representative images and quantification of macrophage tissue inhibitor of metalloproteinase (TIMP)-3 expression as assessed by immunofluorescence staining of brachiocephalic artery plaques from scrambled control and miR-181b inhibitor-treated *Apoe*$^{-/-}$ mice, n=6 to 8/group, **P*<0.05, 2-tailed Student *t* test, scale bar represents 50 µm and is applicable to both panels. **B**, Representative images and quantification of proteolytic activity as assessed by in situ zymography of brachiocephalic plaques from scrambled control and miR-181b inhibitor-treated *Apoe*$^{-/-}$ mice, incubated with substrate alone or plus 10 nmol/L recombinant TIMP-3, #*P*<0.05 and represents significant difference from substrate alone; n=6 to 8 per group, ***P*<0.01 and denotes significant difference from scrambled control mice, ANOVA, scale bar represents 50 µm and is applicable to all panels. **C**, Representative images and quantification of (**D**) plaque cross-sectional area in elastin van Gieson (EVG)–stained sections, (**E**) ratio of total lesional vascular smooth muscle cells (VSMC) and macrophages (Mac) assessed by immunohistochemistry, (**F**) lesional collagen content assessed by picrosirius red staining, (**G**) lesional necrotic core area, (**H**) lesional proliferation percentage determined by immunohistochemistry for proliferating cell nuclear antigen (PCNA), (**I**) lesional apoptosis percentage determined by immunohistochemistry for cleaved caspase-3 (CC3), (**J**) the plaque vulnerability index (necrotic core area+macrophage content/VSMC+collagen content), (**K**) lesional elastin content assessed by EVG staining, in brachiocephalic plaques from scrambled control and miR-181b inhibitor-treated *Apoe*$^{-/-}$ mice, n=6 to 8/group, **P*<0.05 and ***P*<0.01 compared with scrambled control mice, 2-tailed Student *t* test, scale bar in ii represents 100 µm and is applicable to panels i and ii, scale bar in iii represents 100 µm and is applicable to panels iii–viii, scale bar in ix represents 50 µm and is applicable to panels ix–xii. Arrows in panel's ix–xii indicate positive cells. In all cases, data represent the mean±SEM.

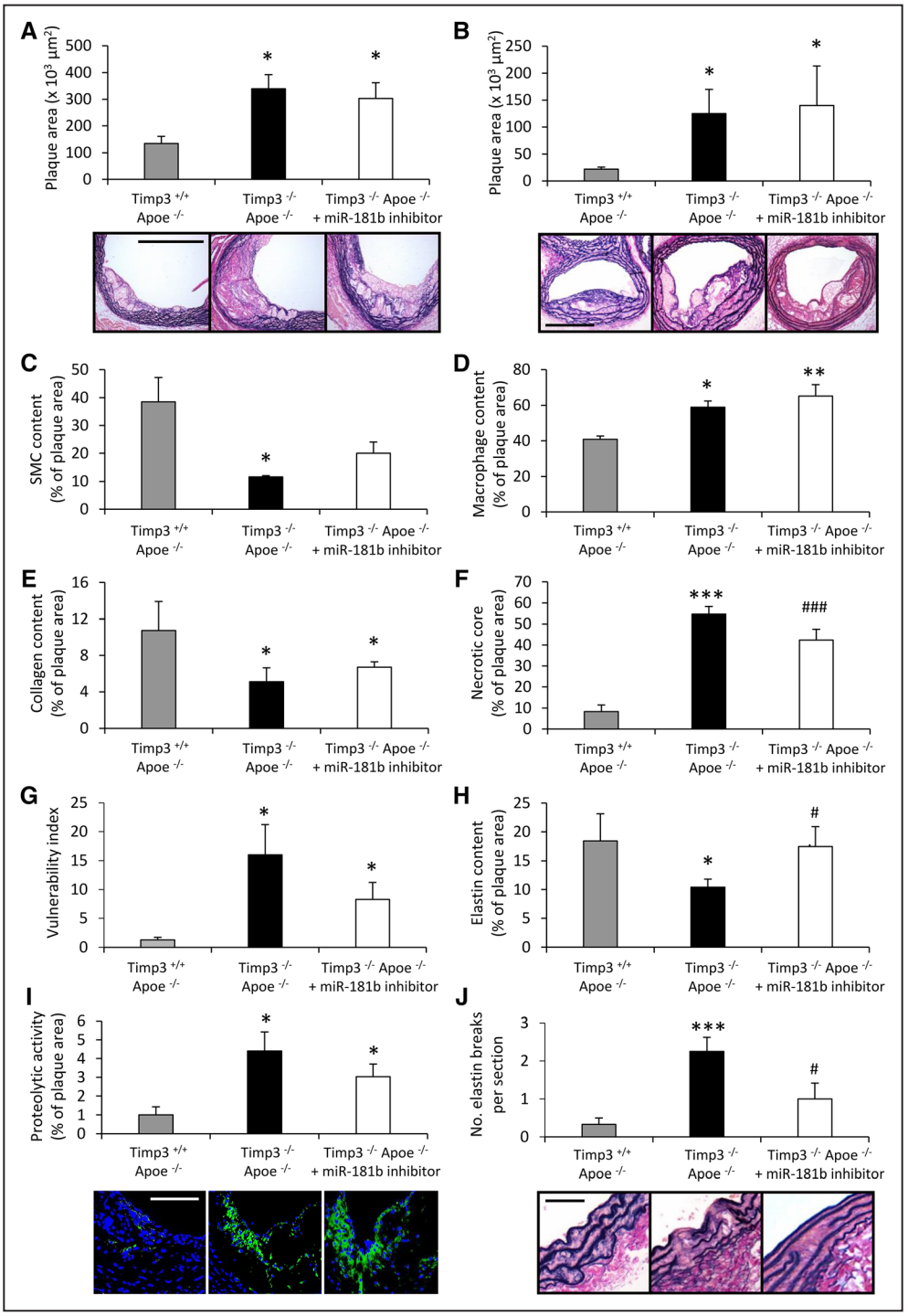

Figure 3. MicroRNA (miR)-181b inhibition does not affect plaque progression in the absence of tissue inhibitor of metalloproteinase (TIMP)-3. Representative images and quantification of plaque cross-sectional area in elastin van Gieson (EVG)–stained sections of plaques within (**A**) the aortic root or (**B**) the brachiocephalic artery of *Timp3*$^{+/+}$ *Apoe*$^{-/-}$, *Timp3*$^{-/-}$ *Apoe*$^{-/-}$, and miR-181b inhibitor-treated *Timp3*$^{-/-}$ *Apoe*$^{-/-}$ mice, n=6 to 8/group, **P*<0.05 and ***P*<0.01 compared with *Timp3*$^{+/+}$ *Apoe*$^{-/-}$ control animals, ANOVA, scale bar represents 100 µm and is applicable to all panels. Quantification of (**C**) smooth muscle cell (SMC), (**D**) macrophage, (**E**) collagen content, (**F**) necrotic core area, (**G**) plaque vulnerability index (necrotic core area+macrophage content/vascular smooth muscle cell+collagen content), and (**H**) elastin content, in brachiocephalic plaques from *Timp3*$^{+/+}$ *Apoe*$^{-/-}$, *Timp3*$^{-/-}$ *Apoe*$^{-/-}$, and miR-181b inhibitor-treated *Timp3*$^{-/-}$ *Apoe*$^{-/-}$ mice, n=6 to 8/group, **P*<0.05, ****P*=0.00013, and ###*P*=0.00938 compared with *Timp3*$^{+/+}$ *Apoe*$^{-/-}$ control animals and #*P*<0.05 compared with *Timp3*$^{-/-}$ *Apoe*$^{-/-}$ mice, ANOVA. **I**, Representative images and quantification of proteolytic activity as assessed by in situ zymography of brachiocephalic plaques from *Timp3*$^{+/+}$ *Apoe*$^{-/-}$, *Timp3*$^{-/-}$ *Apoe*$^{-/-}$, and miR-181b inhibitor-treated *Timp3*$^{-/-}$ *Apoe*$^{-/-}$ mice, n=6 to 8/group, **P*<0.05 compared with *Timp3*$^{+/+}$ *Apoe*$^{-/-}$ control animals, ANOVA, scale bar represents 50 µm and is applicable to all panels. **J**, Representative images and quantification of elastin breaks assessed by EVG staining of brachiocephalic plaques from *Timp3*$^{+/+}$ *Apoe*$^{-/-}$, *Timp3*$^{-/-}$ *Apoe*$^{-/-}$, and miR-181b inhibitor-treated *Timp3*$^{-/-}$ *Apoe*$^{-/-}$ mice, n=6 to 8/group, ****P*=0.0010 compared with *Timp3*$^{+/+}$ *Apoe*$^{-/-}$ control animals and #*P*<0.05 compared with *Timp3*$^{-/-}$ *Apoe*$^{-/-}$ mice, ANOVA. Scale bar represents 25 µm and is applicable to all panels. In all cases, data represent the mean±SEM.

mice (Figure 3A and 3B). Characterization of brachiocephalic artery atherosclerotic plaques from *Timp3*$^{-/-}$/*Apoe*$^{-/-}$ mice revealed that they contained fewer smooth muscle cells (by 70%; $P<0.05$), but increased macrophage content (by 44%; $P<0.05$), than in plaques from *Timp3*$^{+/+}$/*Apoe*$^{-/-}$ control mice (Figure 3C and 3D). Furthermore, whereas there was a reduction in plaque collagen content (by 52%; $P<0.05$), necrotic core area was markedly increased (6.6-fold; $P<0.01$) in plaques from *Timp3*$^{-/-}$/*Apoe*$^{-/-}$ mice compared with those from control animals (Figure 3E and 3F). Collectively, these findings indicate that pathological markers indicative of increased plaque instability in humans are prominent in *Timp3*$^{-/-}$/*Apoe*$^{-/-}$ mice plaques. Indeed, assessment of the vulnerability index showed that this indicator of instability is significantly greater in *Timp3*$^{-/-}$/*Apoe*$^{-/-}$ mice (12-fold; $P<0.05$) compared with *Timp3*$^{+/+}$/*Apoe*$^{-/-}$ control mice (Figure 3G). Consistent with a lack of effect on plaque area, miR-181b inhibition failed to modulate plaque components, such as smooth muscle cell, macrophage, and collagen content, or necrotic core size in *Timp3*$^{-/-}$/*Apoe*$^{-/-}$ mice (Figure 3), in direct contrast to the beneficial effects observed in miR-181b inhibitor-treated *Apoe*$^{-/-}$ mice (Figure 2). Accordingly, the vulnerability index was unaffected in *Timp3*$^{-/-}$/*Apoe*$^{-/-}$ mice by miR-181b inhibition (Figure 3G). Surprisingly, although plaque elastin content was, as expected, decreased in *Timp3*$^{-/-}$/*Apoe*$^{-/-}$ mice (by 43%; $P<0.05$) compared with *Timp3*$^{+/+}$/*Apoe*$^{-/-}$ control mice (Figure 3H), elastin content was restored to levels comparable with control animals, by miR-181b inhibitor treatment of *Timp3*$^{-/-}$/*Apoe*$^{-/-}$ mice (Figure 3H). In situ zymography demonstrated that plaque proteolytic activity was significantly increased in *Timp3*$^{-/-}$/*Apoe*$^{-/-}$ mice (4.4-fold; $P<0.05$) compared with controls and was unaffected by miR-181b inhibition (Figure 3I), implying that the effect of miR-181b inhibition on plaque elastin was, in part, independent of altered proteolysis. Moreover, whereas it was observed that elastin fragmentation was more prevalent within brachiocephalic arteries from *Timp3*$^{-/-}$/*Apoe*$^{-/-}$ mice (6.8-fold; $P<0.0010$) compared with *Timp3*$^{+/+}$/*Apoe*$^{-/-}$ control mice (Figure 3J), miR-181b inhibition reduced the number of elastin breaks in *Timp3*$^{-/-}$/*Apoe*$^{-/-}$ mice (by 66%; $P<0.05$), although still significantly greater in number than *Timp3*$^{+/+}$/*Apoe*$^{-/-}$ control mice (Figure 3J). Together, these data indicate that the majority of the beneficial actions of miR-181b inhibition on existing atherosclerotic plaques are through restoring macrophage TIMP-3 expression, as most effects were abolished in mice with *Timp3* deficiency. However, modulation of plaque elastin content and fragmentation suggest TIMP-3–independent effects of miR-181b inhibition, implying that miR-181b may regulate other targets during atherosclerosis that influence elastin content. Thus, miR-181b inhibition may have a protective role in other vascular pathologies, particularly aneurysms.

MiR Inhibition Stabilizes AAAs in Angiotensin II–Infused *Apoe*$^{-/-}$ Mice

Using the angiotensin II (Ang II)–induced model of AAA formation in *Apoe*$^{-/-}$ mice fed a high-fat diet,[20] we investigated the potential beneficial effects of miR-181b inhibition on the progression of infrarenal atherosclerotic AAAs by using the protocol described in Online Figure X. Treatment with an miR-181b inhibitor did not alter mean arterial blood pressure levels in response to Ang II infusion (Figure 4A) but significantly reduced the occurrence of AAAs to 48% from 86% in scrambled inhibitor-infused, control mice (Figure 4B). Other differences noted included the following: decreased AAA severity (Figure 4C), lowered abdominal aortic miR-181b expression by quantitative polymerase chain reaction (40%; Figure 4D), increased TIMP-3 protein expression (Figure 4E), significantly smaller mean maximal abdominal aortic diameters from histology (Figure 4F and 4G), and markedly more elastin (Figure 4G and 4H). Prominent breaks and fragmentation of the elastic lamellae, key features of AAAs, were abrogated in miR-181b inhibitor-treated compared with control animals (Figure 4I) in association with increased collagen accumulation (by 88%; Figure 4J and 4K). By polarimetry, accumulation of red collagen fibers was greater in AAA tissues from miR-181b inhibitor-treated than control mice, indicating thicker and larger collagen fibrils[21] (Figure 4K). Consistent with the findings in atherosclerotic mice and in line with previous in vitro data showing impaired migration,[8] macrophage content was diminished in AAAs from miR-181b inhibitor-treated mice compared with scrambled control animals (Figure 4L and 4M), associated with marked suppression of macrophage proliferation rates and apoptotic frequencies (87% and 66% respectively; $P<0.05$; Figure 4L, 4N, and 4O). These results demonstrate that administration of an miR-181b inhibitor augments TIMP-3 expression in AAAs, and this is associated with fewer and more stable aneurysms.

MiR-181b Inhibition Regulates Matrix Composition at Other Aneurysmal Sites and Is Protective in an Additional Mouse Model

Aortic aneurysms are subdivided anatomically into thoracic aortic aneurysms and AAAs, and although there are some differences in the underlying pathogenesis, both are characterized by fragmented and diminished elastin fibers.[22] We therefore investigated whether miR-181b inhibition prevents aneurysm formation within the ascending and descending thoracic aortae in our Ang II–infused, *Apoe*$^{-/-}$ mouse model. Mean maximal diameter of descending thoracic aortas in miR-181b inhibitor-treated mice was significantly smaller than those of controls (31%, $P<0.05$; Figure 5A and 5B). The elastin content was also increased together with a decreased number of elastin breaks (Figure 5C and 5D and Online Figure XI). Similar to AAAs, collagen accumulation, particularly more mature collagen fibrils, was increased (Figure 5E). In the ascending thoracic aortas, miR-181b inhibitor-treated mice had decreased vessel expansion compared with controls (by 28%, $P<0.05$; Figure 5F and 5G), which was associated with increased elastin content and reduced elastin fragmentation (Figure 5H and 5I and Online Figure XI). Macrophages were rarely observed at these sites, and TIMP-3 expression was low. Furthermore, no differences in macrophage numbers or TIMP-3 expression were detected between groups (Online Figure XII). These findings show that miR-181b inhibition exerts protective effects on aneurysm formation/progression at multiple susceptible sites within the aorta, even in the absence of overt inflammation, implying additional beneficial

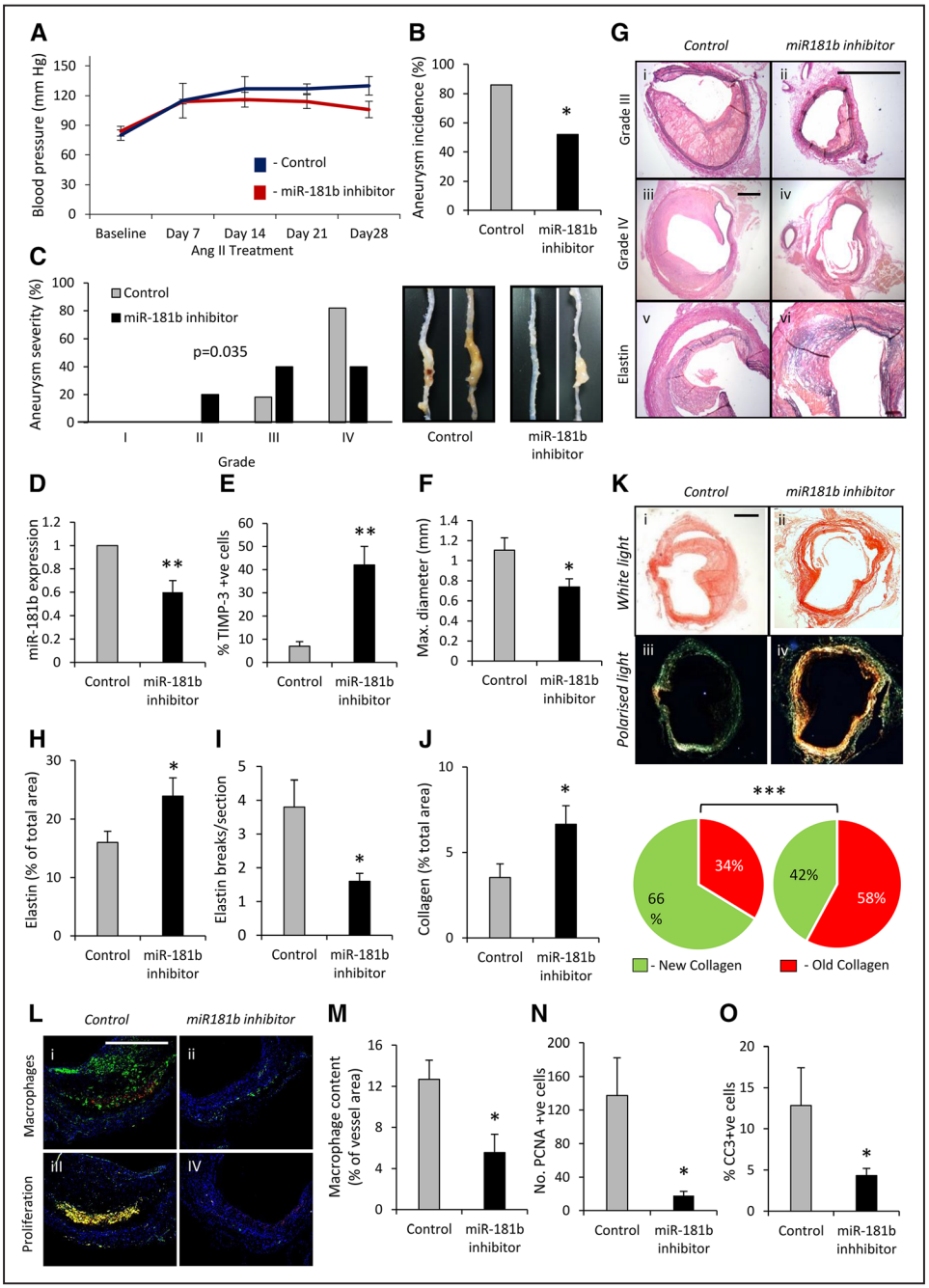

Figure 4. MicroRNA (miR) inhibition stabilizes abdominal aortic aneurysms (AAAs) in angiotensin II-infused *Apoe*$^{-/-}$ mice. A, miR-181b inhibition did not alter blood pressure levels. **B**, Quantification of aneurysm incidence and (**C**) severity (increasing severity from stage I to stage IV as described by Raffort et al[12]) in both groups of mice, using Fisher exact test and 2-tailed Student *t* test, respectively, n=6 to 8/group, **P*<0.05. **D**, Quantification of miR-181b expression by quantitative polymerase chain reaction (Q-PCR) and (**E**) tissue inhibitor of metalloproteinase (TIMP)-3 protein expression by immunohistochemistry, n=6 to 8/group, ***P*<0.01 compared with scrambled control mice, 2-tailed Student *t* test. **F**, Maximal abdominal aortic diameter (mm) within the indicated groups, n=6 to 8/group, ***P*<0.05 compared with scrambled control mice, 2-tailed Student *t* test. **G**, Representative images of elastin van Gieson–stained histological cross-sections of AAAs from scrambled control and miR-181b inhibitor-treated *Apoe*$^{-/-}$ mice, demonstrating the differences in vessel diameter and elastin content (black), scale bar in ii represents 100 μm and is applicable to panels i, ii, and iv–x. Scale bar in iii represents 200 μm and is applicable to panels iii and iv. **H**, Quantification of elastin content and (**I**) elastin breaks in elastin van Gieson–stained AAAs, n=6 to 8/group, **P*<0.05 compared with scrambled control mice, 2-tailed Student *t* test. **J**, Quantification of total collagen content in AAAs assessed by picrosirius red staining, n=6 to 8/group, **P*<0.05 compared with scrambled control mice, 2-tailed Student *t* test. **K**, Representative picrosirius red staining viewed under white light and linearly polarized light to show fibrillar collagen in AAAs of scrambled control and miR-181b inhibitor-treated *Apoe*$^{-/-}$ mice (scale bar in i represents 200 μm and is applicable to all panels), and associated qualitative analysis of new (green) and old (red) fibrillar collagen fiber content, n=6 to 8/group, **P*<0.001 compared with scrambled control mice, Fisher exact test. **L**, Representative images and quantification of (**M**) macrophage content (**N**) proliferation percentage determined by immunohistochemistry for proliferating cell nuclear antigen (PCNA), and (**O**) apoptosis percentage determined by immunohistochemistry for cleaved caspase-3 (CC3), in AAAs from scrambled control and miR-181b inhibitor-treated *Apoe*$^{-/-}$ mice, n=6 to 8/group, **P*<0.05 compared with scrambled control mice, 2-tailed Student *t* test, scale bar in i represents 100 μm and is applicable to all panels. In all cases, data represent the mean±SEM.

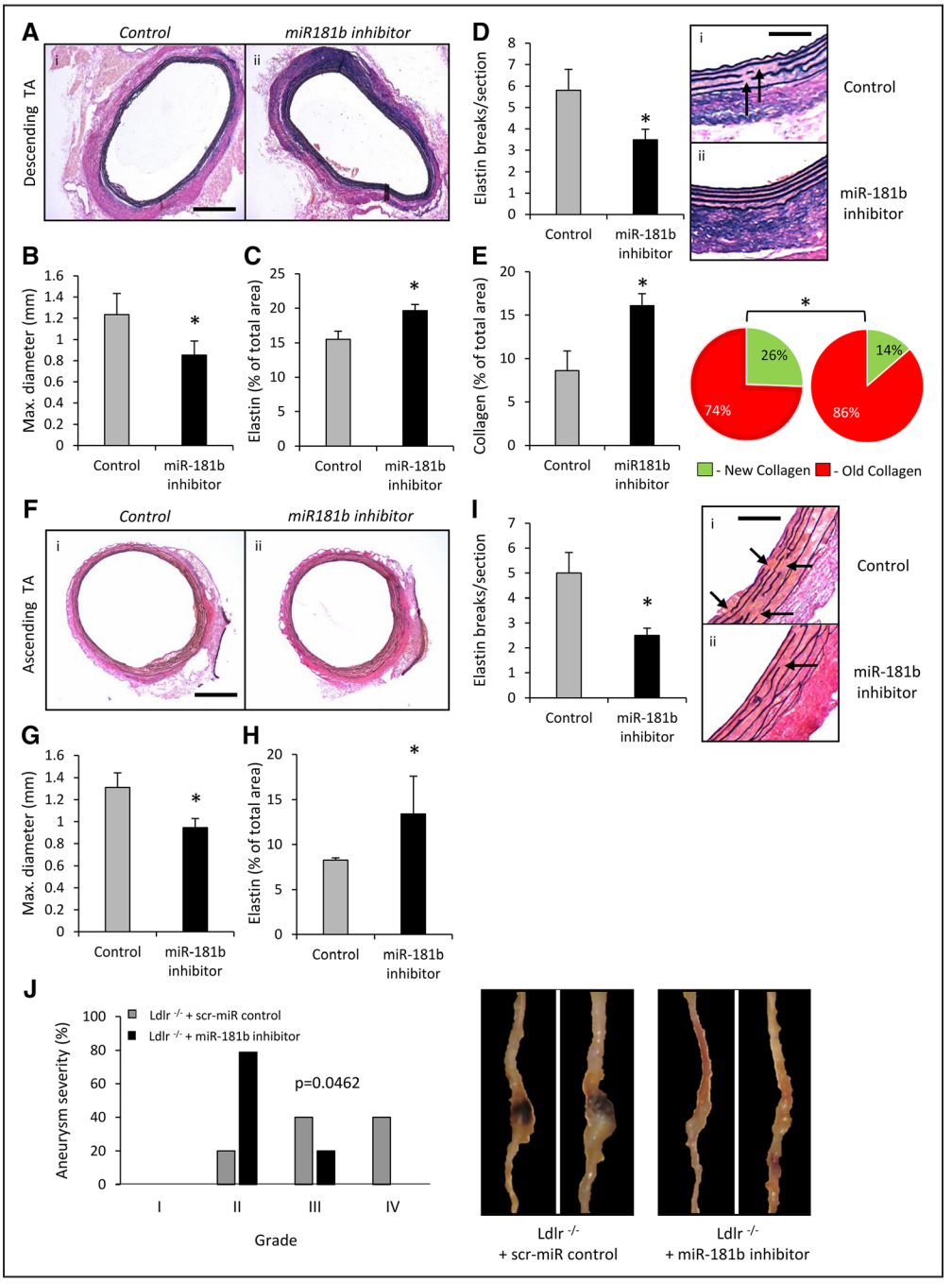

Figure 5. MicroRNA (miR)-181b inhibition regulates matrix composition at other aneurysmal sites and is protective in an additional mouse model. **A**, Representative images and quantification of elastin van Gieson–stained histological cross-sections of descending thoracic aortas (TAs) from scrambled control and miR-181b inhibitor-treated *Apoe*$^{-/-}$ mice demonstrating the differences in (**B**) vessel diameter and (**C**) elastin content (black), n=6 to 8/group, **P*<0.05 compared with scrambled control mice, 2-tailed Student *t* test scale bar in i represents 200 μm and is applicable to both panels. **D**, Quantification of elastin breaks in elastin van Gieson–stained descending TAs, n=6 to 8/group, ***P*<0.01 compared with scrambled control mice, 2-tailed Student *t* test, scale bar in i represents 25 μm and is applicable to both panels, arrows indicate areas of elastin fragmentation. **E**, Quantification of total collagen content and associated qualitative analysis of new (green) and old (red) fibrillar collagen fiber content in descending TAs assessed by picrosirius red staining, n=6 to 8/group, **P*<0.05 compared with scrambled control mice, 2-tailed Student *t* test and Fisher exact test, respectively. **F**, Representative images and quantification of elastin van Gieson–stained histological cross-sections of ascending TAs from scrambled control and miR-181b inhibitor-treated *Apoe*$^{-/-}$ mice, demonstrating the differences in (**G**) vessel diameter and (**H**) elastin content (black), n=6 to 8/group, **P*<0.05 compared with scrambled control mice, 2-tailed Student *t* test scale bar in i represents 200 μm and is applicable to both panels. **I**, Quantification of elastin breaks in elastin van Gieson–stained ascending TAs, n=6 to 8/group, ***P*<0.01 compared with scrambled control mice, 2-tailed Student *t* test, scale bar in i represents 25 μm and is applicable to both panels, arrows indicate areas of elastin fragmentation. **J**, Quantification and associated representative images of aneurysm severity (increasing severity from stage I to stage IV as described by Raffort et al[12]) in scrambled control and miR-181b inhibitor-treated *Ldlr*$^{-/-}$ mice, using Fisher exact test, n=6 to 8/group, **P*<0.05.

effects of miR-181b inhibition independent of increased TIMP-3 protein expression.

To investigate whether the beneficial effects of miR-181b inhibition extended beyond *Apoe*$^{-/-}$ mice, we assessed AAA formation in Ang II–infused, high-fat–fed *Ldlr*$^{-/-}$ mice. AAA severity was significantly reduced in miR-181b inhibitor-treated mice (Figure 5J) compared with scrambled control animals, which exhibited marked aneurysm formation.

MiR-181b Inhibition Mitigates the Progression of Preexisting AAAs in *Apoe*$^{-/-}$ or *Ldlr*$^{-/-}$ Mice

To explore the therapeutic potential of miR-181b inhibition, we next investigated its ability to retard the progression of preexisting AAAs. Consequently, hypercholesterolemic male *Apoe*$^{-/-}$ or *Ldlr*$^{-/-}$ mice undergoing Ang II infusion were treated after development of AAAs, according to the protocol shown in Online Figure VA. AAAs from miR-181b inhibitor-treated *Apoe*$^{-/-}$ mice were notably less dilated than those from controls (Figure 6A and 6B). Further expansion in the average baseline maximal diameter before miR-181b inhibition was significantly decreased by miR-181b inhibition compared with scrambled miR control mice (Figure 6C). Moreover, miR-181b inhibitor significantly increased elastin content, as (Figure 6D and Online Figure VI) and reduced the frequency of elastin fragmentation (Figure 6E and Online Figure VI). Similar favorable outcomes were observed in *Ldlr*$^{-/-}$ mice; aneurysm severity, aortic diameter, and associated vessel expansion were all reduced by miR-181b inhibitor treatment (Figure 6F–6H and Online Figure XI). Similarly, the elastin content of AAAs was increased, whereas elastin breaks were reduced relative to controls (Figure 6I and 6J and Online Figure XI). Hence, miR-181b inhibition can also prevent the progression of preexisting AAAs, while increasing the elastin content of advanced AAAs.

TIMP-3 Protects From Sudden Death Because of Aortic Dissection or Aneurysm Rupture in *Apoe*$^{-/-}$ Mice

To further investigate the role of TIMP-3 in AAA development, *Timp3*$^{-/-}$/*Apoe*$^{-/-}$ and *Timp3*$^{+/+}$/*Apoe*$^{-/-}$ mice were compared in the Ang II–infused high-fat–fed model. Interestingly, whereas 25% of Ang II–infused *Timp3*$^{+/+}$/*Apoe*$^{-/-}$ mice experienced sudden death related to aortic rupture/dissection, the mortality rate of *Timp3*$^{-/-}$/*Apoe*$^{-/-}$ mice was more than doubled (55%, $P<0.01$; Figure 7A). The majority (64%) of *Timp3*$^{-/-}$/*Apoe*$^{-/-}$ mice experienced aortic rupture–related sudden death after 4 to 6 days of Ang II infusion (Figure 7A). Histological examination of AAAs from surviving 28-day Ang II–infused animals revealed that AAA maximal diameter did not differ between groups (Figure 7B), although the average wall thickness was significantly decreased in *Timp3*$^{-/-}$/*Apoe*$^{-/-}$ mice compared with *Timp3*$^{+/+}$/*Apoe*$^{-/-}$ animals (Figure 7C and 7D). *Timp3*$^{-/-}$/*Apoe*$^{-/-}$ mice exhibited decreased elastin content and a greater number of elastin breaks compared with *Timp3*$^{+/+}$/*Apoe*$^{-/-}$ mice (Figure 7D–7F). Moreover, elastin abundance surrounding the aneurysmal sac was less evident in AAAs from *Timp3*$^{-/-}$/*Apoe*$^{-/-}$ mice (Figure 7D). Analysis of AAAs after 7 days Ang II infusion, when rupture and associated death was most prominent in *Timp3*$^{-/-}$/*Apoe*$^{-/-}$ mice, revealed that the ratio of macrophages to smooth muscle cells and markers of apoptosis (p53 and Bax), both characteristics associated with advanced AAAs, were increased relative to *Timp3*$^{+/+}$/*Apoe*$^{-/-}$ mice (Figure 7G–7I). These findings support a critical role for TIMP-3 in AAA rupture that is associated with elastin loss.

Inhibition of miR-181b Attenuates Mortality Rates in *Timp3*$^{-/-}$/*Apoe*$^{-/-}$ Mice by Directly Stimulating Elastin Expression in VSMCs and AAAs

To test whether miR-181b inhibition protects from AAA progression through TIMP-3, we used *Timp3*$^{-/-}$/*Apoe*$^{-/-}$ mice. Contrary to our expectations, inhibition of miR-181b significantly reduced death rates (from 55% to 25%, $P<0.01$; Figure 8A) after >14 days of Ang II infusion. However, AAA severity and incidence were unaffected (Figure 8B), and no differences in AAA maximal diameter, collagen content, or number of elastin breaks were detected (Figure 8C–8E). Interestingly, elastin content was increased in AAAs of miR-181b inhibitor-treated *Timp3*$^{-/-}$/*Apoe*$^{-/-}$ mice (Figure 8F and 8G), implying that miR-181b modulates elastin expression within AAAs, in part independently from TIMP-3. Using an online database (www.targetscan.org), we identified that mature miR-181b can target both mouse and human elastin mRNA at the 3′-untranslated region (Figure 8H). Indeed, using a wild-type elastin-3′-untranslated region reporter expression vector, we observed that the miR-181b inhibitor increased promoter activity ($P<0.01$; Figure 8I). Considering that vessel wall vascular smooth muscle cells (VSMCs) are the predominant source of elastin production, the effect of miR-181b inhibition on this was assessed. Addition of an miR-181b inhibitor to aortic VSMCs significantly increased elastin protein expression (2.6-fold, $P<0.01$; Figure 8J). Addition of Ang II to VSMCs in culture did not modulate miR-181b expression (Online Figure XIII), implying an indirect effect of Ang II, such as in response to hypertension. Taken together, these findings demonstrate that miR-181b inhibition exerts a dual protective role on AAA progression, through augmenting TIMP-3 expression and directly increasing elastin expression.

Discussion

The accumulation of macrophages, heightened proteolytic activity, and loss of matrix proteins are considered pivotal events during the progression and rupture of atherosclerotic plaques and aneurysms. We demonstrate here, for the first time, that miR-181b exacerbates these processes and consequently promotes inflammatory cardiovascular diseases. First, we show that miR-181b mediates the downregulation by GM-CSF of macrophage TIMP-3 protein expression. Second, macrophage TIMP-3 protein expression is reduced alongside increased miR-181b levels in both advanced human atherosclerotic plaques and AAAs. Third, miR-181b through TIMP-3 downregulation is a key regulator of numerous macrophage functions involved in plaque and aneurysm progression, including increased MMP activity, macrophage invasion and accumulation, proliferation, and apoptosis. Finally, and most importantly, miR-181b inhibition decreases atherosclerotic plaque formation in mouse models, primarily through upregulation of macrophage TIMP-3 expression, whereas in aneurysm

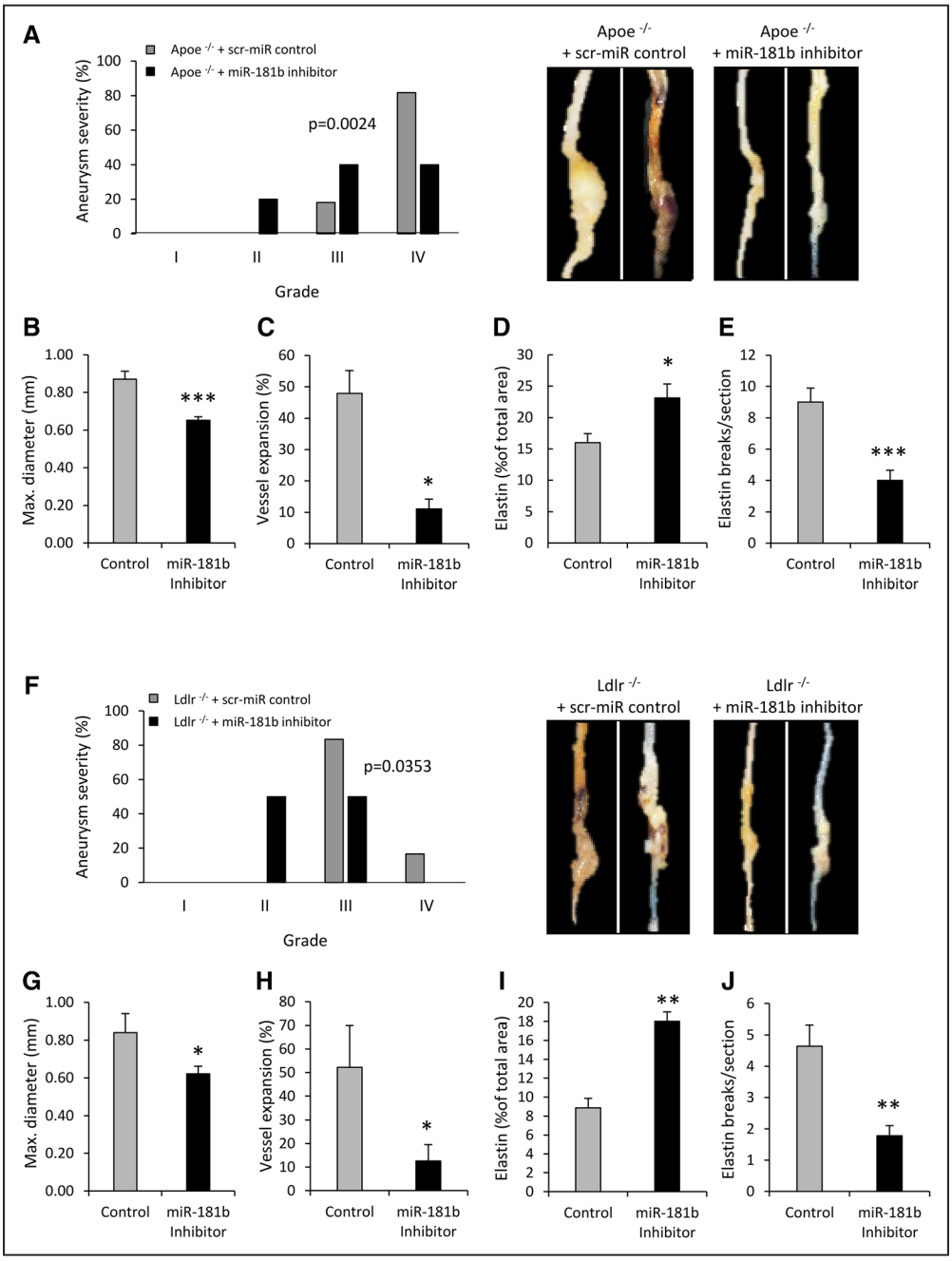

Figure 6. MicroRNA (miR)-181b inhibition mitigates the progression of preexisting abdominal aortic aneurysms (AAAs) in *Apoe*$^{-/-}$ or *Ldlr*$^{-/-}$ mice. **A**, Quantification and associated representative images of aneurysm severity (increasing severity from stage I to stage IV as described by Raffort et al[12]) in scrambled control and miR-181b inhibitor-treated *Apoe*$^{-/-}$ mice with preexisting AAAs, using Fisher exact test, n=6 to 7/group. Quantification of (**B**) vessel diameter, (**C**) vessel expansion, (**D**) elastin content, and (**E**) elastin breaks in scrambled control and miR-181b inhibitor-treated *Apoe*$^{-/-}$ mice with preexisting AAAs, n=6 to 7/group, **P*<0.05 and ****P*=0.0007 compared with scrambled control mice, 2-tailed Student *t* test. **F**, Quantification and associated representative images of aneurysm severity (increasing severity from stage I to stage IV as described by Raffort et al[12]) in scrambled control and miR-181b inhibitor-treated *Ldlr*$^{-/-}$ mice with preexisting AAAs, using Fisher exact test, n=6 to 7/group. Quantification of (**G**) vessel diameter, (**H**) vessel expansion, (**I**) elastin content, and (**J**) elastin breaks in scrambled control and miR-181b inhibitor-treated *Ldlr*$^{-/-}$ mice with preexisting AAAs, n=6 to 7/group, **P*<0.05 and ***P*<0.01 compared with scrambled control mice, 2-tailed Student *t* test.

models there is an additional effect on elastin production from VSMC that is supported by in vitro studies. Concomitantly, the composition of atherosclerotic plaques and AAAs is favorably altered and exhibits characteristics associated with stable plaques[23] and aneurysms[4] in man. Taken together, these findings imply a dual beneficial effect of miR-181b inhibition during atherosclerosis and AAAs, namely increased macrophage TIMP-3 protein expression and heightened VSMC elastin production, which could eventually be exploited therapeutically.

The progression and rupture of atherosclerotic plaques and AAAs underlie the majority of cardiovascular-related

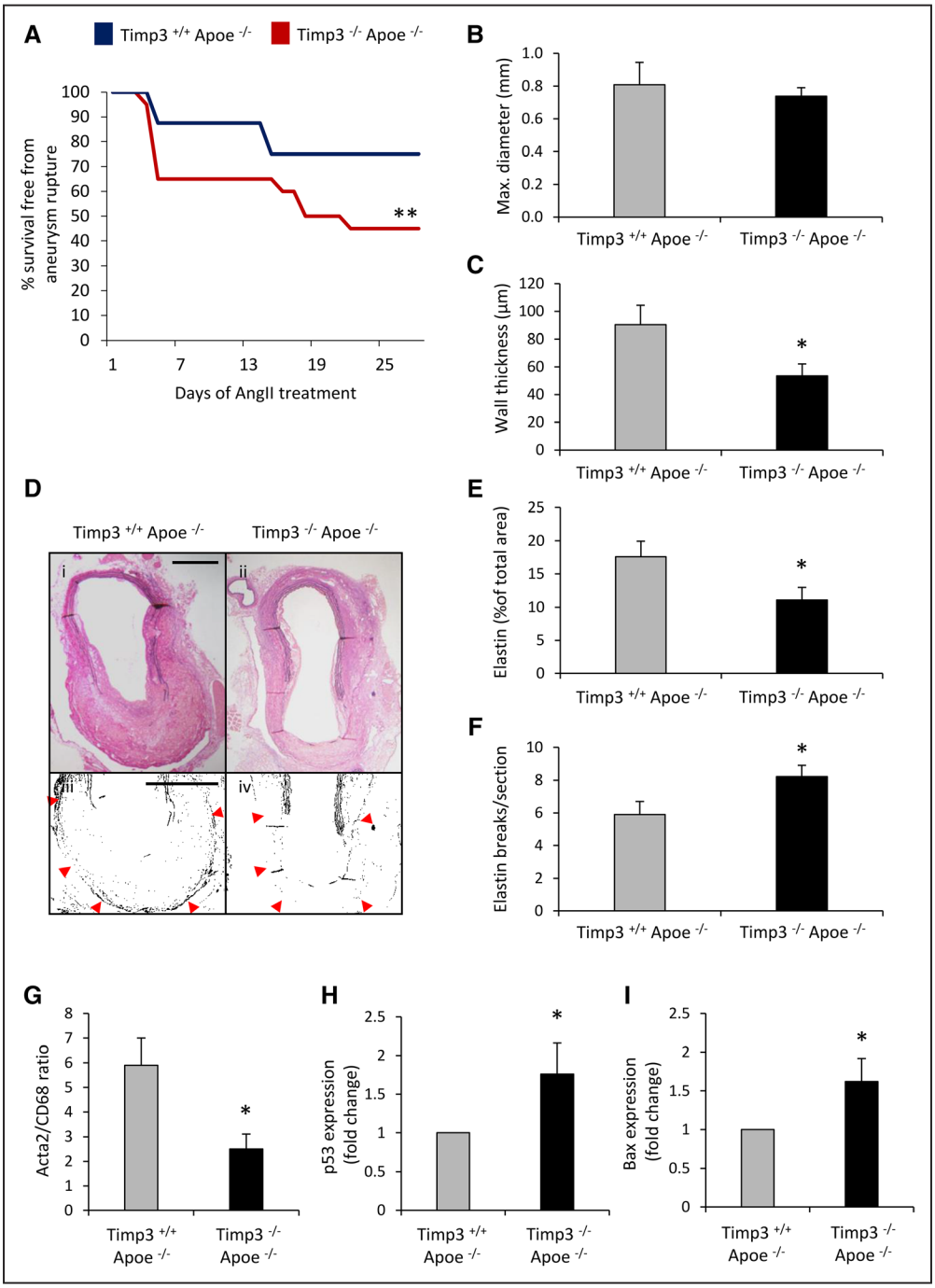

Figure 7. Tissue inhibitor of metalloproteinase (TIMP)-3 protects from sudden death because of aortic dissection or aneurysm rupture in *Apoe*$^{-/-}$ mice. **A**, Kaplan–Meier curves of survival free from aneurysm rupture in 28 days Ang II–infused hypercholesterolemic *Timp3*$^{+/+}$ *Apoe*$^{-/-}$ and *Timp3*$^{-/-}$ *Apoe*$^{-/-}$ mice, n=15 to 20/group. Quantification of (**B**) vessel diameter and (**C**) average wall thickness in *Timp3*$^{+/+}$ *Apoe*$^{-/-}$ and *Timp3*$^{-/-}$ *Apoe*$^{-/-}$ mice, n=6 to 8/group. **D**, Representative elastin van Gieson–stained abdominal aortic aneurysms (AAAs; i and ii) and higher magnification monochrome images (iii and iv) from *Timp3*$^{+/+}$ *Apoe*$^{-/-}$ and *Timp3*$^{-/-}$ *Apoe*$^{-/-}$ mice and associated quantification of elastin content (**E**) and fragmentation (**F**). Scale bars represent 200 µm, and red arrows depict external elastic lamellae. Quantification of (**G**) smooth muscle cell (acta2) to macrophage (CD68) ratio, (**H**) p53, and (**I**) Bax expression in *Timp3*$^{+/+}$ *Apoe*$^{-/-}$ and *Timp3*$^{-/-}$ *Apoe*$^{-/-}$ mice with preexisting AAAs, n=6 to 8/group. Statistical comparisons were made using log-rank test (**A**) or 2-tailed Student *t* test (**B–I**), **P*<0.05 and ***P*<0.01 compared with *Timp3*$^{+/+}$ *Apoe*$^{-/-}$ mice. In all cases, data represent the mean±SEM.

deaths. Elucidating novel pathogenetic factors, such as miR-181b, is therefore paramount for the development of efficient new therapies. Human pathological observations suggest that ECM disruption caused by persistent inflammation drives the formation and progression of atherosclerotic plaques and AAAs, particularly the transition of asymptomatic plaques and small dilatations to clinically relevant plaques and large AAA ruptures.[4,5] Furthermore, a wealth of mechanistic investigations and studies in relevant animal models have highlighted the critical role of MMPs in collagen and elastin

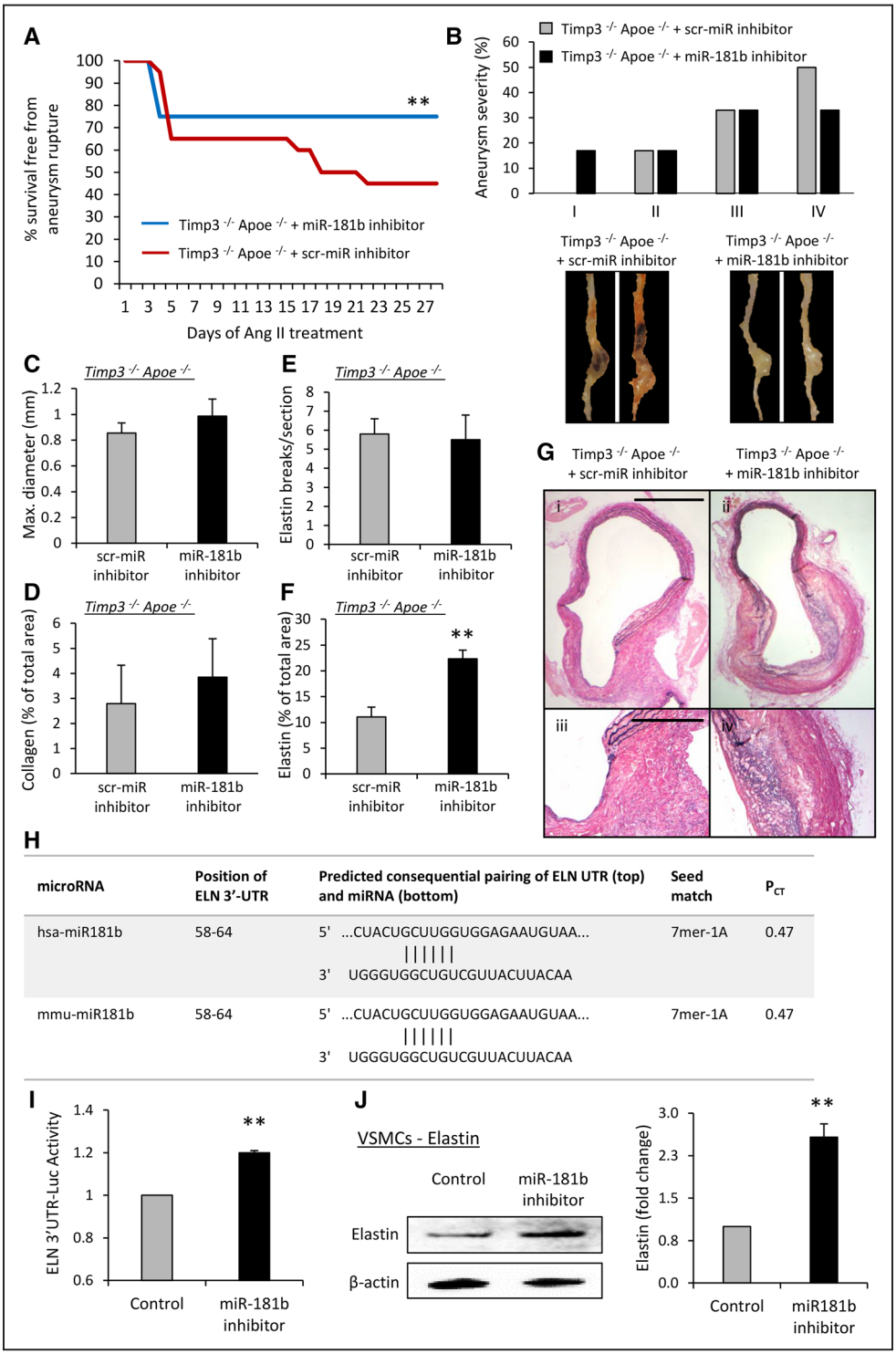

Figure 8. Inhibition of microRNA (miR)-181b attenuates mortality rates in *Timp3*$^{-/-}$/*Apoe*$^{-/-}$ mice by directly stimulating elastin expression in vascular smooth muscle cells (VSMCs) and abdominal aortic aneurysms (AAAs). A, Kaplan–Meier curves of survival free from aneurysm rupture in control and miR-181b inhibitor-treated Ang II–infused hypercholesterolemic *Timp3*$^{-/-}$ *Apoe*$^{-/-}$ mice, n=10 to 20/group. **B**, Quantification and associated representative images of aneurysm severity in control and miR-181b inhibitor-treated *Timp3*$^{-/-}$ *Apoe*$^{-/-}$ mice, n=6 to 7/group. Quantification of (**C**) vessel diameter, (**D**) collagen content, (**E**) elastin breaks, (**F**) elastin content, and (**G**) representative images of elastin van Gieson–stained AAAs from control and miR-181b inhibitor-treated *Timp3*$^{-/-}$ *Apoe*$^{-/-}$ mice, n=6 to 7/group, scale bar in i represents 200 μm and is applicable to panels i and ii, scale bar in ii represents 100 μm and is applicable to panels iii and iv. **H**, Conserved miR-181b–binding sites of the 3′-untranslated region (3′-UTR) of human (hsa) and murine (mmu) elastin (*ELN*). P_{CT} refers to the probability of preferentially conserved targeting, demonstrating miR-181b preferentially targets *ELN* in both species. **I**, 3′-UTR luciferase reporter activity of human *ELN* in HeLa cells treated with an miR-181b inhibitor or a scrambled control, n=6. **J**, Representative Western blot and quantification of elastin protein expression in human aortic smooth muscle cells after addition of an miR-181b inhibitor or a scrambled control, n=4. Statistical comparisons were made using log-rank test (**A**), Fisher exact test (**B**), or 2-tailed Student *t* test (**C**–**J**), **P*<0.05, ***P*<0.01, and ***P*<0.01 compared with controls. In all cases, data represent the mean±SEM.

degradation, culminating in atherosclerotic plaque destabilization and medial destruction of the aneurysm wall.[7,17,24–27] Conversely, TIMPs, by limiting proteolytic activity against ECM and inflammation-related proteins, undoubtedly have protective roles in the progression of atherosclerosis and AAAs.[5] Although both reduce atherosclerosis and aneurysm formation in mouse models,[28] TIMP-2 seems to play a greater protective role than TIMP-1 in both atherosclerosis[29] and aneurysm formation.[30] The beneficial effect of TIMP-2 is in part through suppression of monocyte/macrophage MMP-14 expression/activity, leading to reduced invasion and accumulation.[29] MMP-14 (also known as MT1 [membrane type I]-MMP) is inhibited by TIMP-2 and also TIMP-3, but poorly by TIMP-1.[31] Consistent with this, MMP-14–mediated monocyte/macrophage transmigration across an endothelial monolayer in vitro is efficiently blocked by TIMP-2 and -3, whereas TIMP-1 is ineffective.[32] TIMP-3 is distinct from TIMP-2 in 2 important aspects; it binds tightly to the ECM, suggesting that it has a principal role in pericellular proteolysis, and it also targets several members of the ADAMs (disintegrin metalloproteinases) family. Previous studies described protective effects of TIMP-3 during atherogenesis and aortic dilatation in rabbits, as well as mice. Atherosclerotic lesion area at the aortic root was increased in *Timp3*$^{-/-}$/*Apoe*$^{-/-}$ mice, alongside heightened inflammation and decreased collagen content.[33] Conversely, systemic or myeloid cell-specific overexpression of TIMP-3 diminished atherogenesis within an *Apoe*$^{-/-}$ mouse partial carotid artery ligation model[34] or in the aortic root of *Ldlr*$^{-/-}$ mice.[35] Deletion of *Timp3* in C57Bl/6 mice infused with Ang II revealed that TIMP-3 reduces adverse remodeling.[36] Moreover, administration of a broad-spectrum MMP inhibitor rescued vessel enlargement in *Timp3*$^{-/-}$ mice, demonstrating that decreased metalloproteinase activity largely accounted for the protection afforded by TIMP-3.[36] Our current data and supporting studies demonstrate that expression of TIMP-3 at the mRNA level increases dramatically during monocyte to macrophage differentiation, irrespective of whether this occurs in the presence of M-CSF or GM-CSF.[14] However, we demonstrated that a distinct subset of foam cell macrophages (which frequent human atherosclerotic plaques and AAAs) exhibit TIMP-3 downregulation (and concomitant increased MMP-14 protein levels).[8] This unique macrophage phenotype is highly invasive and has increased proliferation and apoptosis rates, all properties expected to destabilize atherosclerotic plaques and AAAs.[8] The aim of the present study was to elucidate the basis for post-translational regulation of TIMP-3 and investigate its impact during the evolution of inflammation-associated atherosclerosis and AAAs, studies that led to the identification and characterization of miR181b.

In addition to arterial dilatation, AAAs are characterized by decreased medial elastin content and disruption or fragmentation of elastic lamellae,[4] and MMPs, especially MMP-12, clearly play an important role in this context.[37–40] Indeed, elastin preservation in the $CaCl_2$ experimental model was observed in aortas of select *Mmp*-knockout mice[38,41] and in mice treated systemically with a c-Jun N-terminal kinase inhibitor to hinder MMP production.[42] Moreover, numerous studies have evaluated the effects of nonspecific MMP inhibitors in organ culture experiments or animal models of AAAs. Animal studies with doxycycline, a tetracycline analogue that reduces the expression and activity of several MMPs, attenuated elastin fragmentation and loss in rodent AAA models.[43–45] Similarly, hydroxamate-based broad-spectrum MMP inhibitors also suppressed elastin degeneration within experimental AAAs in murine models.[46–48] Furthermore, manipulation of individual TIMPs has also demonstrated the ability of these endogenous inhibitors to preserve elastin within the aneurysmal wall.[30,36,49,50] TIMP-3 augmentation achieved through miR-181b inhibition undoubtedly suppresses the activity of MMPs that target elastin, including MMP-12. We demonstrate here that elastin stabilization is also achieved through a direct effect of miR-181b on elastin protein synthesis. Furthermore, increased elastin content associated with miR-181b inhibition was accompanied by a more stable composition of atherosclerotic plaques and aneurysms, including greater collagen accumulation and enhanced smooth muscle cell to macrophage ratio. Similarly, stabilization and preservation of aortic elastin in the $CaCl_2$ AAA model with pentagalloyl glucose prevented aortic dilatation during both development and progression.[51] Impairment of elastin structure through heterozygous or homozygous mutation of the fibrillin-1 (*Fbn1*) gene is also associated with accelerated atherosclerosis[52] and aneurysm rupture.[53] Malformation of mature elastin fibers through fibulin-4 deficiency also results in aortic aneurysms.[54] The above studies alongside our own findings show that elastin preservation is consistently associated with retardation of aneurysm and atherosclerosis progression. This indicates that elastin stabilization by either TIMP-3–directed MMP inhibition or increased elastin synthesis is both afforded by miR-181b inhibition.

Our previous findings[8] and current results imply that regulation of both MMP-14 and TIMP-3 expression is both regulated by post-transcriptional mechanisms and that both are under the control of GM-CSF. GM-CSF increases macrophage MMP-14 levels and activity by suppressing miR-24. Moreover, reduction of miR-24 drives advanced atherosclerotic plaque progression.[10] We show here that GM-CSF sustains miR-181b expression during monocyte-to-macrophage differentiation, and TIMP-3 is therefore inhibited.[10] GM-CSF also increases MMP-12 expression in macrophages, although this occurs at the level of transcription.[55] GM-CSF expression is increased in unstable atherosclerotic plaques,[10,56] and administration of GM-CSF to high-fat–fed *Apoe*$^{-/-}$ mice accelerates atherogenesis.[57] Similarly, GM-CSF is abundant in human and mouse aortic aneurysms.[58] Furthermore, GM-CSF administration induced AAA development[57] and caused aortic dissection[59] in high-fat–fed *Apoe*$^{-/-}$ mice and $CaCl_2$ application/Ang II–infused C57Bl/6 mice, respectively. GM-CSF neutralization abrogated inflammatory aneurysm development and matrix-degrading activity in a *Smad3*$^{-/-}$ mouse model.[58] Clinically, a positive correlation between plasma concentrations of GM-CSF and intracranial aneurysms has been reported,[60] and circulating levels of GM-CSF are also elevated in patients with acute aortic dissection.[59] All of this evidence supports the concept that GM-CSF plays a major part in atherosclerosis and AAAs, in part by sustaining miR-181b

levels. In future experiments beyond the present scope, it will be valuable to investigate these concepts further by manipulating the expression of GM-CSF.

We are aware that miR-181b has many additional predicted targets, which may be involved in the advantageous antiatherosclerotic and antianeurysm effects observed in vivo. However, our in vitro, in vivo, and human pathological experiments demonstrate a dominant role of TIMP-3 in protecting from disease progression subsequent to miR-181b inhibition. It has recently been reported that miR-181b can regulate nuclear factor-κB–mediated activation of endothelial cells and ensuing vascular inflammation.[61] However, effects on atherosclerosis and aneurysm were not assessed, although the authors did demonstrate that miR-181b overexpression in endothelial cells dramatically suppressed TIMP-3 expression.[61] It is also plausible that other miRs can regulate TIMP-3 expression in atherosclerosis and aneurysms, affecting disease development. Indeed, inhibition of miR-712 (or its human homologue miR-205) prevented endothelial inflammation and atherosclerosis in a carotid ligation model[34] and aortic dilatation, elastin fragmentation, and aortic rupture in *Apoe*$^{-/-}$ mice,[62] potentially through post-transcriptional regulation of TIMP-3 and associated heightened MMP activity. In concert with our previous findings[8–10] and the in situ zymography in the present study, we predict that the activity of select MMPs, such as MMP-14, is retarded through miR-181b–dependent TIMP-3 upregulation, although TIMP-3 can inhibit the activity of multiple MMPs, ADAMs, and aggrecanases (ADAMTS-4 and -5), the individual roles/activities of which were not determined in the current study. Nonetheless, our current findings demonstrate that restoration of TIMP-3 levels achieved through miR-181b inhibition retards the progression of atherosclerotic plaques and aneurysms at multiple vascular beds and in different mouse strains. Furthermore, considering that TIMP-3 has been validated as a target of miR-181b,[13] our experiments conducted in *Timp3*–deficient mice strongly imply that the beneficial effects afforded by miR-181b inhibition are largely TIMP-3 dependent during atherosclerosis in *Apoe*$^{-/-}$ mice, although an additional protective effect is achieved through elevating elastin synthesis during formation of AAAs.

A further limitation of our study is the use of cell markers and plaque characteristics to infer the stability of atherosclerotic lesions, considering the unproven assumptions inherent in such definitions. However, plaque composition defined by the content of VSMCs and collagen compared with macrophage and lipid is still referred to in the literature as delineators of plaque vulnerability.[63] Moreover, it has recently been suggested that cells other than macrophages express CD68, which we used as a marker of macrophages in the present study, and subsequently, all mentions to macrophages are in fact CD68^{+ve} cells. Finally, to ensure the reliability of our semiquantitative assessment of histological parameters, intra- and interobserver coefficients were nonsignificant demonstrating that the difference between measurements was within the limits of agreement (Online Figure XIV).

We present here novel in vivo findings that miR-181b inhibition reduces the progression of established atherosclerotic plaques and AAAs, mediated by increased expression of TIMP-3 in intraplaque and intra-aneurysm macrophages and elastin expression in VSMC. Inhibition of miR-181b favorably altered the composition of atherosclerotic plaques and AAAs consistent with improved stability. Furthermore, elevated miR-181b expression occurred in human plaques histologically characterized as stable and correlated with decreased macrophage TIMP-3 expression. Similar results were also observed in human AAA samples when compared with nonaneurysmal aortae. Collectively, these findings support the development of clinically applicable strategies to inhibit miR-181b, thereby maintaining or elevating TIMP-3 and elastin expression, and reducing elastin degradation. Such inhibition of miR-181b could serve as a therapeutic approach in reversing the advancement of atherosclerosis and aortic aneurysms and avoiding the associated acute clinical syndromes.

Sources of Funding

This work was supported by grants from the British Heart Foundation to J. L. Johnson (FS/07/053/24069 and PG/13/48/30341) and support from the National Institute for Health Research Bristol Cardiovascular Biomedical Research Unit.

Disclosures

None.

References

1. Virmani R, Burke AP, Farb A, Kolodgie FD. Pathology of the vulnerable plaque. *J Am Coll Cardiol*. 2006;47:C13–C18. doi: 10.1016/j.jacc.2005.10.065.
2. Newby AC. Metalloproteinases and vulnerable atherosclerotic plaques. *Trends Cardiovasc Med*. 2007;17:253–258. doi: 10.1016/j.tcm.2007.09.001.
3. Dollery CM, Libby P. Atherosclerosis and proteinase activation. *Cardiovasc Res*. 2006;69:625–635. doi: 10.1016/j.cardiores.2005.11.003.
4. Nordon IM, Hinchliffe RJ, Loftus IM, Thompson MM. Pathophysiology and epidemiology of abdominal aortic aneurysms. *Nat Rev Cardiol*. 2011;8:92–102. doi: 10.1038/nrcardio.2010.180.
5. Johnson JL, Newby AC. Macrophage heterogeneity in atherosclerotic plaques. *Curr Opin Lipidol*. 2009;20:370–378. doi: 10.1097/MOL.0b013e3283309848.
6. Johnson JL. Matrix metalloproteinases: influence on smooth muscle cells and atherosclerotic plaque stability. *Expert Rev Cardiovasc Ther*. 2007;5:265–282. doi: 10.1586/14779072.5.2.265.
7. Johnson JL. Matrix metalloproteinases and their inhibitors in cardiovascular pathologies: current knowledge and clinical potential. *Metalloproteinases Med*. 2014;1:21–36.
8. Johnson JL, Sala-Newby GB, Ismail Y, Aguilera CM, Newby AC. Low tissue inhibitor of metalloproteinases 3 and high matrix metalloproteinase 14 levels defines a subpopulation of highly invasive foam-cell macrophages. *Arterioscler Thromb Vasc Biol*. 2008;28:1647–1653. doi: 10.1161/ATVBAHA.108.170548.
9. Johnson JL, Jenkins NP, Huang WC, Di Gregoli K, Sala-Newby GB, Scholtes VP, Moll FL, Pasterkamp G, Newby AC. Relationship of MMP-14 and TIMP-3 expression with macrophage activation and human atherosclerotic plaque vulnerability. *Mediators Inflamm*. 2014;2014:276457. doi: 10.1155/2014/276457.
10. Di Gregoli K, Jenkins N, Salter R, White S, Newby AC, Johnson JL. MicroRNA-24 regulates macrophage behavior and retards atherosclerosis. *Arterioscler Thromb Vasc Biol*. 2014;34:1990–2000. doi: 10.1161/ATVBAHA.114.304088.
11. Feinberg MW, Moore KJ. MicroRNA regulation of atherosclerosis. *Circ Res*. 2016;118:703–720. doi: 10.1161/CIRCRESAHA.115.306300.
12. Raffort J, Lareyre F, Clement M, Mallat Z. Micro-RNAs in abdominal aortic aneurysms: insights from animal models and relevance to human disease. *Cardiovasc Res*. 2016;110:165–177. doi: 10.1093/cvr/cvw046.
13. Wang B, Hsu SH, Majumder S, Kutay H, Huang W, Jacob ST, Ghoshal K. TGFbeta-mediated upregulation of hepatic miR-181b promotes

hepatocarcinogenesis by targeting TIMP3. *Oncogene*. 2010;29:1787–1797. doi: 10.1038/onc.2009.468.
14. Fabunmi RP, Sukhova GK, Sugiyama S, Libby P. Expression of tissue inhibitor of metalloproteinases-3 in human atheroma and regulation in lesion-associated cells: a potential protective mechanism in plaque stability. *Circ Res*. 1998;83:270–278.
15. Tsarouhas K, Soufla G, Apostolakis S, Zaravinos A, Panagiotou M, Khoury M, Hassoulas JA, Tsatsakis AM, Spandidos DA. Transcriptional regulation of TIMPs in ascending aorta aneurysms. *Thromb Res*. 2010;126:399–405. doi: 10.1016/j.thromres.2010.08.015.
16. Ogata T, Shibamura H, Tromp G, Sinha M, Goddard KA, Sakalihasan N, Limet R, MacKean GL, Arthur C, Sueda T, Land S, Kuivaniemi H. Genetic analysis of polymorphisms in biologically relevant candidate genes in patients with abdominal aortic aneurysms. *J Vasc Surg*. 2005;41:1036–1042. doi: 10.1016/j.jvs.2005.02.020.
17. Ikonomidis JS, Jones JA, Barbour JR, Stroud RE, Clark LL, Kaplan BS, Zeeshan A, Bavaria JE, Gorman JH III, Spinale FG, Gorman RC. Expression of matrix metalloproteinases and endogenous inhibitors within ascending aortic aneurysms of patients with Marfan syndrome. *Circulation*. 2006;114:I365–I370. doi: 10.1161/CIRCULATIONAHA.105.000810.
18. Di Gregoli K, Johnson JL. Role of colony-stimulating factors in atherosclerosis. *Curr Opin Lipidol*. 2012;23:412–421. doi: 10.1097/MOL.0b013e328357ca6e.
19. Shiomi M, Ito T, Hirouchi Y, Enomoto M. Fibromuscular cap composition is important for the stability of established atherosclerotic plaques in mature WHHL rabbits treated with statins. *Atherosclerosis*. 2001;157:75–84.
20. Daugherty A, Manning MW, Cassis LA. Angiotensin II promotes atherosclerotic lesions and aneurysms in apolipoprotein E-deficient mice. *J Clin Invest*. 2000;105:1605–1612. doi: 10.1172/JCI7818.
21. Quillard T, Tesmenitsky Y, Croce K, Travers R, Shvartz E, Koskinas KC, Sukhova GK, Aikawa E, Aikawa M, Libby P. Selective inhibition of matrix metalloproteinase-13 increases collagen content of established mouse atherosclerosis. *Arterioscler Thromb Vasc Biol*. 2011;31:2464–2472. doi: 10.1161/ATVBAHA.111.231563.
22. Guo DC, Papke CL, He R, Milewicz DM. Pathogenesis of thoracic and abdominal aortic aneurysms. *Ann N Y Acad Sci*. 2006;1085:339–352. doi: 10.1196/annals.1383.013.
23. Davies MJ. Going from immutable to mutable atherosclerotic plaques. *Am J Cardiol*. 2001;88:2F–9F.
24. Galis ZS, Sukhova GK, Lark MW, Libby P. Increased expression of matrix metalloproteinases and matrix degrading activity in vulnerable regions of human atherosclerotic plaques. *J Clin Invest*. 1994;94:2493–2503. doi: 10.1172/JCI117619.
25. Halpert I, Sires UI, Roby JD, Potter-Perigo S, Wight TN, Shapiro SD, Welgus HG, Wickline SA, Parks WC. Matrilysin is expressed by lipid-laden macrophages at sites of potential rupture in atherosclerotic lesions and localizes to areas of versican deposition, a proteoglycan substrate for the enzyme. *Proc Natl Acad Sci U S A*. 1996;93:9748–9753.
26. Libby P. Collagenases and cracks in the plaque. *J Clin Invest*. 2013;123:3201–3203. doi: 10.1172/JCI67526.
27. Hellenthal FA, Buurman WA, Wodzig WK, Schurink GW. Biomarkers of AAA progression. Part 1: extracellular matrix degeneration. *Nat Rev Cardiol*. 2009;6:464–474. doi: 10.1038/nrcardio.2009.80.
28. Xiong W, Knispel R, Mactaggart J, Baxter BT. Effects of tissue inhibitor of metalloproteinase 2 deficiency on aneurysm formation. *J Vasc Surg*. 2006;44:1061–1066. doi: 10.1016/j.jvs.2006.06.036.
29. Johnson JL, Baker AH, Oka K, Chan L, Newby AC, Jackson CL, George SJ. Suppression of atherosclerotic plaque progression and instability by tissue inhibitor of metalloproteinase-2: involvement of macrophage migration and apoptosis. *Circulation*. 2006;113:2435–2444. doi: 10.1161/CIRCULATIONAHA.106.613281.
30. Di Gregoli K, George SJ, Jackson CL, Newby AC, Johnson JL. Differential effects of tissue inhibitor of metalloproteinase (TIMP)-1 and TIMP-2 on atherosclerosis and monocyte/macrophage invasion. *Cardiovasc Res*. 2016;109:318–330. doi: 10.1093/cvr/cvv268.
31. English JL, Kassiri Z, Koskivirta I, Atkinson SJ, Di Grappa M, Soloway PD, Nagase H, Vuorio E, Murphy G, Khokha R. Individual Timp deficiencies differentially impact pro-MMP-2 activation. *J Biol Chem*. 2006;281:10337–10346. doi: 10.1074/jbc.M512009200.
32. Sithu SD, English WR, Olson P, Krubasik D, Baker AH, Murphy G, D'Souza SE. Membrane-type 1-matrix metalloproteinase regulates intracellular adhesion molecule-1 (ICAM-1)-mediated monocyte transmigration. *J Biol Chem*. 2007;282:25010–25019. doi: 10.1074/jbc.M611273200.
33. Stöhr R, Cavalera M, Menini S, Mavilio M, Casagrande V, Rossi C, Urbani A, Cardellini M, Pugliese G, Menghini R, Federici M. Loss of TIMP3 exacerbates atherosclerosis in ApoE null mice. *Atherosclerosis*. 2014;235:438–443. doi: 10.1016/j.atherosclerosis.2014.05.946.
34. Son DJ, Kumar S, Takabe W, Kim CW, Ni CW, Alberts-Grill N, Jang IH, Kim S, Kim W, Won Kang S, Baker AH, Woong Seo J, Ferrara KW, Jo H. The atypical mechanosensitive microRNA-712 derived from pre-ribosomal RNA induces endothelial inflammation and atherosclerosis. *Nat Commun*. 2013;4:3000. doi: 10.1038/ncomms4000.
35. Casagrande V, Menghini R, Menini S, et al. Overexpression of tissue inhibitor of metalloproteinase 3 in macrophages reduces atherosclerosis in low-density lipoprotein receptor knockout mice. *Arterioscler Thromb Vasc Biol*. 2012;32:74–81. doi: 10.1161/ATVBAHA.111.238402.
36. Basu R, Fan D, Kandalam V, Lee J, Das SK, Wang X, Baldwin TA, Oudit GY, Kassiri Z. Loss of Timp3 gene leads to abdominal aortic aneurysm formation in response to angiotensin II. *J Biol Chem*. 2012;287:44083–44096. doi: 10.1074/jbc.M112.425652.
37. Luttun A, Lutgens E, Manderveld A, Maris K, Collen D, Carmeliet P, Moons L. Loss of matrix metalloproteinase-9 or matrix metalloproteinase-12 protects apolipoprotein E-deficient mice against atherosclerotic media destruction but differentially affects plaque growth. *Circulation*. 2004;109:1408–1414. doi: 10.1161/01.CIR.0000121728.14930.DE.
38. Longo GM, Buda SJ, Fiotta N, Xiong W, Griener T, Shapiro S, Baxter BT. MMP-12 has a role in abdominal aortic aneurysms in mice. *Surgery*. 2005;137:457–462. doi: 10.1016/j.surg.2004.12.004.
39. Wang Y, Ait-Oufella H, Herbin O, Bonnin P, Ramkhelawon B, Taleb S, Huang J, Offenstadt G, Combadière C, Rénia L, Johnson JL, Tharaux PL, Tedgui A, Mallat Z. TGF-beta activity protects against inflammatory aortic aneurysm progression and complications in angiotensin II-infused mice. *J Clin Invest*. 2010;120:422–432. doi: 10.1172/JCI38136.
40. Johnson JL, Devel L, Czarny B, George SJ, Jackson CL, Rogakos V, Beau F, Yiotakis A, Newby AC, Dive V. A selective matrix metalloproteinase-12 inhibitor retards atherosclerotic plaque development in apolipoprotein E-knockout mice. *Arterioscler Thromb Vasc Biol*. 2011;31:528–535. doi: 10.1161/ATVBAHA.110.219147.
41. Longo GM, Xiong W, Greiner TC, Zhao Y, Fiotti N, Baxter BT. Matrix metalloproteinases 2 and 9 work in concert to produce aortic aneurysms. *J Clin Invest*. 2002;110:625–632. doi: 10.1172/JCI15334.
42. Yoshimura K, Aoki H, Ikeda Y, Furutani A, Hamano K, Matsuzaki M. Regression of abdominal aortic aneurysm by inhibition of c-Jun N-terminal kinase in mice. *Ann N Y Acad Sci*. 2006;1085:74–81. doi: 10.1196/annals.1383.031.
43. Boyle JR, McDermott E, Crowther M, Wills AD, Bell PR, Thompson MM. Doxycycline inhibits elastin degradation and reduces metalloproteinase activity in a model of aneurysmal disease. *J Vasc Surg*. 1998;27:354–361.
44. Petrinec D, Liao S, Holmes DR, Reilly JM, Parks WC, Thompson RW. Doxycycline inhibition of aneurysmal degeneration in an elastase-induced rat model of abdominal aortic aneurysm: preservation of aortic elastin associated with suppressed production of 92 kD gelatinase. *J Vasc Surg*. 1996;23:336–346.
45. Curci JA, Petrinec D, Liao S, Golub LM, Thompson RW. Pharmacologic suppression of experimental abdominal aortic aneurysms: acomparison of doxycycline and four chemically modified tetracyclines. *J Vasc Surg*. 1998;28:1082–1093.
46. Prescott MF, Sawyer WK, Von Linden-Reed J, Jeune M, Chou M, Caplan SL, Jeng AY. Effect of matrix metalloproteinase inhibition on progression of atherosclerosis and aneurysm in LDL receptor-deficient mice overexpressing MMP-3, MMP-12, and MMP-13 and on restenosis in rats after balloon injury. *Ann N Y Acad Sci*. 1999;878:179–190.
47. Moore G, Liao S, Curci JA, Starcher BC, Martin RL, Hendricks RT, Chen JJ, Thompson RW. Suppression of experimental abdominal aortic aneurysms by systemic treatment with a hydroxamate-based matrix metalloproteinase inhibitor (RS 132908). *J Vasc Surg*. 1999;29:522–532.
48. Bigatel DA, Elmore JR, Carey DJ, Cizmeci-Smith G, Franklin DP, Youkey JR. The matrix metalloproteinase inhibitor BB-94 limits expansion of experimental abdominal aortic aneurysms. *J Vasc Surg*. 1999;29:130–138; discussion 138.
49. Eskandari MK, Vijungco JD, Flores A, Borensztajn J, Shively V, Pearce WH. Enhanced abdominal aortic aneurysm in TIMP-1-deficient mice. *J Surg Res*. 2005;123:289–293. doi: 10.1016/j.jss.2004.07.247.
50. Allaire E, Forough R, Clowes M, Starcher B, Clowes AW. Local overexpression of TIMP-1 prevents aortic aneurysm degeneration and rupture in a rat model. *J Clin Invest*. 1998;102:1413–1420. doi: 10.1172/JCI2909.

51. Isenburg JC, Simionescu DT, Starcher BC, Vyavahare NR. Elastin stabilization for treatment of abdominal aortic aneurysms. *Circulation*. 2007;115:1729–1737. doi: 10.1161/CIRCULATIONAHA.106.672873.
52. Van Herck JL, De Meyer GR, Martinet W, Van Hove CE, Foubert K, Theunis MH, Apers S, Bult H, Vrints CJ, Herman AG. Impaired fibrillin-1 function promotes features of plaque instability in apolipoprotein E-deficient mice. *Circulation*. 2009;120:2478–2487. doi: 10.1161/CIRCULATIONAHA.109.872663.
53. Carta L, Pereira L, Arteaga-Solis E, Lee-Arteaga SY, Lenart B, Starcher B, Merkel CA, Sukoyan M, Kerkis A, Hazeki N, Keene DR, Sakai LY, Ramirez F. Fibrillins 1 and 2 perform partially overlapping functions during aortic development. *J Biol Chem*. 2006;281:8016–8023. doi: 10.1074/jbc.M511599200.
54. Huang J, Davis EC, Chapman SL, Budatha M, Marmorstein LY, Word RA, Yanagisawa H. Fibulin-4 deficiency results in ascending aortic aneurysms: a potential link between abnormal smooth muscle cell phenotype and aneurysm progression. *Circ Res*. 2010;106:583–592. doi: 10.1161/CIRCRESAHA.109.207852.
55. Wu L, Tanimoto A, Murata Y, Fan J, Sasaguri Y, Watanabe T. Induction of human matrix metalloproteinase-12 gene transcriptional activity by GM-CSF requires the AP-1 binding site in human U937 monocytic cells. *Biochem Biophys Res Commun*. 2001;285:300–307. doi: 10.1006/bbrc.2001.5161.
56. Sugiyama S, Okada Y, Sukhova GK, Virmani R, Heinecke JW, Libby P. Macrophage myeloperoxidase regulation by granulocyte macrophage colony-stimulating factor in human atherosclerosis and implications in acute coronary syndromes. *Am J Pathol*. 2001;158:879–891. doi: 10.1016/S0002-9440(10)64036-9.
57. Haghighat A, Weiss D, Whalin MK, Cowan DP, Taylor WR. Granulocyte colony-stimulating factor and granulocyte macrophage colony-stimulating factor exacerbate atherosclerosis in apolipoprotein E-deficient mice. *Circulation*. 2007;115:2049–2054. doi: 10.1161/CIRCULATIONAHA.106.665570.
58. Ye P, Chen W, Wu J, Huang X, Li J, Wang S, Liu Z, Wang G, Yang X, Zhang P, Lv Q, Xia J. GM-CSF contributes to aortic aneurysms resulting from SMAD3 deficiency. *J Clin Invest*. 2013;123:2317–2331. doi: 10.1172/JCI67356.
59. Son BK, Sawaki D, Tomida S, Fujita D, Aizawa K, Aoki H, Akishita M, Manabe I, Komuro I, Friedman SL, Nagai R, Suzuki T. Granulocyte macrophage colony-stimulating factor is required for aortic dissection/intramural haematoma. *Nat Commun*. 2015;6:6994. doi: 10.1038/ncomms7994.
60. Chalouhi N, Theofanis T, Starke RM, Zanaty M, Jabbour P, Dooley SA, Hasan D. Potential role of granulocyte-monocyte colony-stimulating factor in the progression of intracranial aneurysms. *DNA Cell Biol*. 2015;34:78–81. doi: 10.1089/dna.2014.2618.
61. Sun X, Icli B, Wara AK, Belkin N, He S, Kobzik L, Hunninghake GM, Vera MP, Blackwell TS, Baron RM, Feinberg MW; MICU Registry. MicroRNA-181b regulates NF-κB-mediated vascular inflammation. *J Clin Invest*. 2012;122:1973–1990. doi: 10.1172/JCI61495.
62. Kim CW, Kumar S, Son DJ, Jang IH, Griendling KK, Jo H. Prevention of abdominal aortic aneurysm by anti-microRNA-712 or anti-microRNA-205 in angiotensin II-infused mice. *Arterioscler Thromb Vasc Biol*. 2014;34:1412–1421. doi: 10.1161/ATVBAHA.113.303134.
63. Bentzon JF, Otsuka F, Virmani R, Falk E. Mechanisms of plaque formation and rupture. *Circ Res*. 2014;114:1852–1866. doi: 10.1161/CIRCRESAHA.114.302721.

Novelty and Significance

What Is Known?

- Rupture of atherosclerotic plaques and abdominal aortic aneurysms underlies most cardiovascular-related deaths.
- Progressive accumulation of macrophages contributes to the pathogenesis of atherosclerosis and aneurysms.
- Macrophages at rupture-prone sites of plaques and aneurysms display increased expression and activity of several matrix metalloproteinases but decreased expression of tissue inhibitor of matrix metalloproteinases (TIMP)-3.

What New Information Does This Article Contribute?

- TIMP-3 is reduced in plaque and aneurysm macrophages during disease progression because of negative regulation by the proatherogenic and proaneurysmal microRNA (miR)-181b.
- Inhibition of miR-181b protects against atherosclerosis and aortic aneurysm through increasing expression levels of macrophage TIMP-3 and vascular smooth muscle cell elastin.
- TIMP-3 deficiency promotes atherosclerosis and aortic aneurysm formation and reduces the beneficial effects of miR-181b inhibition.

An imbalance between matrix metalloproteinases and TIMPs, resulting in heightened proteolytic activity, occurs in advanced atherosclerotic plaques and abdominal aortic aneurysms. In addition, a macrophage phenotype defined by decreased expression of TIMP-3 is associated with increased matrix degradation. Consequently, novel methods to promote the expression of TIMP-3 are desirable. In this study, we show that genetic deletion of TIMP-3 results in more advanced atherosclerotic plaques and aortic aneurysms. Moreover, we discover that miR-181b regulates macrophage TIMP-3 expression and that while miR-181b increases during the progression of atherosclerotic plaques and aneurysms, TIMP-3 protein expression diminishes. Accordingly, inhibition of miR-181b in multiple mouse models exerts antiatherosclerotic and antianeurysmal effects, predominantly through increasing macrophage TIMP-3 expression and vascular smooth muscle cell elastin levels. These findings demonstrate that TIMP-3 is protective toward atherosclerosis and aneurysm formation and that targeting miR-181b may provide a novel strategy for limiting the progression of atherosclerotic plaques and aortic aneurysms.

Circulation Research
JOURNAL OF THE AMERICAN HEART ASSOCIATION

MicroRNA-181b Controls Atherosclerosis and Aneurysms Through Regulation of TIMP-3 and Elastin

Karina Di Gregoli, Nur Najmi Mohamad Anuar, Rosaria Bianco, Stephen J. White, Andrew C. Newby, Sarah J. George and Jason L. Johnson

Circ Res. 2017;120:49-65; originally published online October 18, 2016;
doi: 10.1161/CIRCRESAHA.116.309321
Circulation Research is published by the American Heart Association, 7272 Greenville Avenue, Dallas, TX 75231

Print ISSN: 0009-7330. Online ISSN: 1524-4571

Supplemental Material

Methods

Human coronary and aortic samples

Coronary artery segments were collected from cadaveric heart donors from the Bristol Valve Bank, and incorporated into the Bristol Coronary Artery Biobank under National Research Ethics Service approval (08/H0107/48). Valve donor patients had died of non-cardiac related pathologies, and from the limited information retrieved under our ethics, were not prescribed statins or other known athero-modifying medications. The average age of patients with histologically defined stable and unstable plaques was 56±2 and 59±2 years, respectively and a 6/4 male to female ratio. Human aneurysmal abdominal aortic samples and non-aneurysmal aortic specimens were collected under National Research Ethics Service approval (11/H0102/3). Q-CPR for miR-181b was conducted and data analysed after normalization to Scarna17 expression and CD68 mRNA expression. Paraffin sections from histologically classified stable or unstable coronary artery plaques alongside aneurysmal and non-aneurysmal aortas, were stained with a CD68 antibody to detect macrophages and a TIMP-3 antibody, and the percentage of TIMP-3 positive macrophages quantified.

In situ hybridisation

For the detection of miR-181b in human stable and unstable coronary atherosclerotic plaques, 3µm serial sections were subjected to in situ hybridisation (ISH). In brief, cleared slides were underwent citrate buffer-induced antigen retrieval and subsequent immersion in 0.2M HCl for 20 minutes. After three washes in 0.3% triton-X, slides were incubated with 15µg proteinase K at 37°C for 20 minutes then fixed with 3% PFA for 10 minutes. Following incubation with hybridisation buffer (50% formamide, 4 x SSC, 2.5 x Denhadrt's solution, 2.5mg/ml salmon DNA, 0.6mg/ml yeast tRNA, 0.025% SDS and 0.1% blocking reagent) at 60°C for 1 hour slides were incubated with 70µl of 40nM 5', 3' double digoxigenin-labeled locked nucleic acid (LNA)-modified miRCURY miR-181b detection probe or scrambled miRCURY LNA oligonucleotide to serve as a negative control (Exiqon, Denmark), in the same buffer at 60°C overnight. After stringency washing with different concentrations of SSC buffer and blocking for 1 hour (1% blocking reagent in PBS and 10% FCS), HRP-conjugated mouse monoclonal antibody to digoxigenin (DIG) (Abcam) diluted in 1x blocking buffer at a concentration of 1:200 was added for 1 hour. After washing (0.1M Tris PH 9.0), AlexaFluor-594-labelled tyramide (Invitrogen) was added to each section and incubated in the dark at room temperature for 1 hour. After washing slides were mounted with ProLong Gold with Dapi (Invitrogen). The number of miR-181b positive macrophages as assessed by CD68 staining on serial sections, was assessed and expressed as percentage of $CD68^{+}$ cells positive for mir-181b..

Animals

Timp3 $^{-/-}$ mice (FVB/N strain background)were provided by Professor Dylan Edwards (University of East Anglia) (1). Apoe $^{-/-}$ and Ldlr $^{-/-}$ mice (both C57Bl/6N strain background) were purchased from the Jackson Laboratory and maintained within our own animal facility. Apoe $^{-/-}$ mice were crossed with Timp3 $^{-/-}$ mice to generate Timp3 $^{-/-}$/Apoe $^{-/-}$ double knockout mice as well as their relevant age-, strain-, and sex-matched Timp3 $^{+/+}$/Apoe $^{-/-}$ single knockout littermate controls.

Atherosclerosis studies

In order to assess effects on established atherosclerotic lesions within the brachiocephalic arteries of Apoe $^{-/-}$ mice, female animals at the age of 8-10 weeks were fed a high-fat diet containing 21% (wt : wt) pork lard and supplemented with 0.15% (wt : wt) cholesterol (Special Diet Services, Witham, UK) for 12 weeks, as previously demonstrated (2). Due to Ldlr $^{-/-}$ mice exhibiting milder total cholesterol levels and associated slower plaque development than their Apoe $^{-/-}$ counterparts (3), 8-10 week old male Ldlr $^{-/-}$ mice were high-fat fed for 14 weeks to induce the formation of intermediate plaques. The above experimental plans are illustrated in Supplementary Figure VI.

Mouse model of Ang II–induced aortic aneurysm

To induce AAA formation in atherosclerotic plaque-prone Apoe $^{-/-}$ or Ldlr $^{-/-}$ mice, male animals at the age of 8-10 weeks were fed a high-fat diet containing 21% (wt : wt) pork lard and supplemented with 0.15% (wt : wt) cholesterol (Special Diet Services, Witham, UK) for 8 weeks, the last four weeks of which they were infused with Ang II as previously described (4). The above experimental plans are illustrated in Supplementary Figure X. Alzet model 1007D, 1002 and 1004 osmotic mini-pumps (Charles River UK) implanted subcutaneously were used to deliver Ang II (500 or 1000 ng/kg/min, Enzo Life Sciences), for 7, 14, or 28 days, depending on the experimental design. Mice were anaesthetised with isoflurane and oxygen (2.5% and 1L/min) which was followed by mini-pump implantation. Post-operative analgesia was performed by intraperitoneal injection of buprenorphine (0.1mg/kg), immediately after surgery and animals closely monitored for 24 hours and subsequent pain relief delivered if necessary. To ensure that the studies were adequately powered, group sizes of at least 10 animals were used per group, accepting a 15-20% attrition rate due to early aortic rupture and sudden death. To assess the incidence and severity of AAA formation, the method outlined by Daugherty and colleagues was adopted (5). Aneurysms were graded based on the following scale: Type I, dilated lumen in the supra-renal region of the aorta with no thrombus. Type II, remodelled tissue in the supra-renal region that frequently contains thrombus. Type III, a pronounced bulbous form of type II that contains thrombus. Type IV, a form in which there are multiple aneurysms containing thrombus, some overlapping, in the suprarenal area of the aorta. Aneurysmal tissue was categorized independently by two blinded observers. There was complete concordance in the designation by the two observers.

In vivo miR-181b inhibition

Atherosclerosis study: 8 mg/kg dose of either a LNA-anti-miR181b or scrambled (scr)-miR (miR-CURY LNA miR inhibitor from Exiqon) was injected via the tail vein of high fat-fed Apoe $^{-/-}$ or Ldlr $^{-/-}$ mice (as previously described (6)). Injection was repeated after 4 days and sample collected 3 days after the second injection. Aneurysm study: 4 mg/kg dose of either a LNA-anti-miR181b or scr-miR was delivered by intraperitoneal injection of high fat-fed Apoe $^{-/-}$ or Ldlr $^{-/-}$ mice at the same time as Ang II delivery commenced (to assess effects on AAA development), or 28 days after Ang II-infusion (to assess effects on AAA progression). In both instances injections were repeated weekly, for four weeks for the AAA development study, and two weeks for the AAA progression study.

Termination

Animals were anaesthetised by intraperitoneal injection of sodium pentobarbitone (500mg/kg), before exsanguination by perfusion via the heart with PBS at a constant pressure of 100 mmHg, with outflow through the incised jugular veins. This was followed by constant pressure perfusion with 10% formalin for at least 5 minutes.

Cholesterol Assay

Cholesterol levels from mouse plasma were quantified using the BioVison Cholesterol Assay Kit (Cambridge BioSciences, Cambridge, UK).

Characterisation of atherosclerotic plaques

Up to four vessel cross-sections were quantified per mouse, between 150 and 200µm apart. Paraffin-embedded brachiocephalic artery sections were used. Elastin staining was visualized using Elastin van Gieson histochemistry for plaque morphometric analysis. Up to five vessel cross-sections were quantified per mouse. Analysis was performed using a computerised image analysis program (Image Pro Plus, DataCell, Maidenhead, UK). The lengths of the internal and external elastic lamellae were recorded by image analysis. These were used to derive the total vessel area and the (lumen + plaque) area, by assuming them to be the circumferences of perfect circles. Plaque area was measured directly, and was subtracted from the area enclosed by the internal elastica to derive the lumen area.

Characterisation of aneurysmal lesions

Up to four vessel cross-sections were quantified per mouse, between 150 and 200µm apart. Paraffin-embedded ascending, descending and abdominal aortic sections were used. Elastin staining was visualized using Elastin van Gieson histochemistry, and the number of degraded elastin lamellae and elastin content was quantified by a researcher blinded to the experimental protocol. Morphometric analysis was performed using a computerised image analysis program (Image Pro Plus, DataCell, Maidenhead, UK). The lengths of the internal and external elastic lamellae were recorded by image analysis. These were used to derive the total vessel area, lumen area, mean wall thickness, and maximum diameter by assuming them to be the circumferences of perfect circles. Plaque area was measured directly, and was subtracted from the area enclosed by the internal elastica to derive the lumen area.

Histological and immunohistochemical analysis

Up to four vessel cross-sections were quantified per mouse, between 150 and 200µm apart. Brachiocephalic artery and aortic sections were cut at 3µm and subjected to the following histo- and immunohisto-chemical analyses. Quantitative analysis of fibrillar collagen content was performed using picrosirius red staining of sections viewed under polarised light. Qualitative analysis of fibre thickness was assessed by delineating green and red fibres disposed under polarised light, as fibre colour variation progresses from green to red proportionally to the increase of fibre thickness/ages, as described previously (7) The relative amount of each fibre colour was expressed as a percentage of the total amount of collagen in the area of interest. Quantitative analysis of elastin content and elastin breaks was performed using elastin van Gieson stained sections (four sections/vessel of interest/animal, 200µm apart). The relative amount of elastin (which appears as black under light microscopy) was determined using a computerised image analysis program (Image Pro Plus, DataCell, Maidenhead, UK) and expressed as an average percentage in the area of interest (plaque or aneurysmal artery), whilst the number of elastin breaks per section were counted and expressed as average number of elastin breaks per section averaged from four sections taken 200µm apart. Sections were subjected to immunohistochemistry for smooth muscle cells (α-smooth muscle actin), macrophages (CD68), TIMP-3, proliferation cell nuclear antigen (PCNA) or cleaved caspase-3 (CC3) as described previously (6). Primary antibody details are listed in Supplemental Table 1. Dual immunohistochemistry was performed by incubating sections with two appropriate primary antibodies simultaneously. Cells stained positive with the cell-specific markers were counted and density expressed as the percentage of total nucleated cells stained positive per plaque, or as percentage of positive area of interest. Vulnerability index was calculated by dividing the percentage of plaque area occupied by macrophages and necrotic core, by that of vascular smooth muscle cells and collagen. A score significantly >1 implies increased vulnerability, conversely significantly <1 suggests heightened stability (8).

In situ zymography

Gelatinolytic activity was localised in arteries removed from *Apoe* knockout mice that had received high-fat diet for 13 weeks treated with a miR-181b inhibitor or scrambled control for the last 7 days, as previously described (6). In brief, frozen 8 µm cryostat sections were incubated overnight at room temperature in a humidified dark chamber with 20 µg/mL DQ™ Gelatin (Life Technologies Ltd, Paisley, UK) dissolved in developing buffer (50 mM Tris, pH 7.4, 150 mM NaCl, 5 mM CaCl2, 0.2 mM sodium azide). Cleavage of the substrate by proteinases results in unblocking of quenched fluorescence and in an increase in fluorescence intensity. Sections were incubated for 24 hours in developing buffer alone, or in the presence of recombinant TIMP-3 (10nM; 973-TM-010; R&D Systems). Sections were washed in PBS, fixed with 4% paraformaldehyde, and mounted with ProLong® Gold antifade reagent with DAPI (Life Technologies Ltd, Paisley, UK). Using fluorescence microscopy, gelatinolytic activity was identified as green fluorescence.

Monocyte Isolation, macrophage maturation, and gene expression analysis

Peripheral blood mononuclear cells were isolated by differential centrifugation from whole blood of healthy donors, which were collected under South West 4 Research Ethics Committee reference 09/H0107/22. Blood (24mL per donor) was diluted with Dulbecco's Phosphate Buffered Saline (PBS) without calcium and magnesium (Lonza) (ratio 1:1). The diluted samples were subjected to density gradient separation on Ficoll Paque Plus (ratio 1:1) (GE Healthcare Life Sciences) and centrifuged. After centrifugation the PBMC layer was collected and washed in Hank's Balanced Salt Sodium (HBSS) with phenol red without calcium and magnesium (Lonza). Monocytes were isolated by adhering the peripheral blood mononuclear cells to tissue culture plastic for 2 hours at a concentration of 2.5×10^6 cells/mL. Monocytes were cultured in RPMI media with 2mM L-glutamine, 100 IU/mL penicillin, 100 µg/mL streptomycin, 10% fetal bovine serum (FBS; Lonza, Sigma), and either 20 ng/mL recombinant human macrophage-colony stimulating factor (M-CSF; R & D systems) or recombinant human granulocyte macrophage-colony stimulating factor (GM-CSF; R & D systems), for 7 days to generate mature macrophages (6). The Qiagen miRNeasy kit was used for total RNA extraction including micro RNA (Qiagen) in accordance with the manufacturer's protocol. Recover-All kit (Ambion) was used for RNA isolation from paraffin-embedded sections according to the manufacturer's instructions. RNA samples were quantified with a NanoDrop ND-1000 spectrophotomter (LabTech International). Equal amounts of cDNA were generated using a miScript Reverse Transcription Kit (Qiagen) Real-time quantitative PCR was performed in a Roche Light Cycler 1.5 to quantify the steady-state concentration of RNA using a QuantiTect SYBR Green PCR Kit and primers as detailed in Supplemental Table II. Samples were incubated first at 42°C for 30 minutes then at 95°C for 3 minutes. The cDNA obtained was stored at -80°C.

Macrophage and vascular smooth muscle cell miR-181b inhibitor transfection

The RVG-9dR peptide (9) was used to deliver anti-has-miR-181b miScript miRNA inhibitor (10nM) or a scrambled control (Qiagen) to 7 day GM-CSF matured macrophages, as described previously (6). Four hours post-transfection in serum free antibiotic free RPMI, the media was changed and fresh RPMI/FCS was added to each sample. Cells were then cultured for 24 hours before collection in SDS lysis buffer. Human aortic vascular smooth muscle cells were cultured in DMEM containing 10% FCS. Cells were transfected with 50nM anti-has-miR-181b miScript miRNA inhibitor (Qiagen) using Lipofectamine RNAiMax (Invitrogen) according to the manufacturer's instructions. Appropriate negative controls were also utilised (0.1 nM All Stars Negative Control (Qiagen). Cells were cultured for at least 24 hours before collection for downstream analysis.

Western Blotting

SDS lysis buffer was used to extract macrophage or VSMC proteins and total protein concentration was measured using a bicinchoninic acid protein assay kit (Pierce). Equal protein concentrations were loaded and electrophoresed on 4-12% gradient gels (Novex Bis-Tris gel) and transferred to 0.2µm nitrocellulose membranes. Blots were blocked with 5% (w/v) skimmed milk powder and incubated overnight at 4^0C with anti-TIMP-3 or anti-elastin antibody (see Supplemental Table I) diluted in SignalBoost™ Solution 1 (Merck). Primary antibodies were detected using species-relevant HRP-conjugated secondary antibodies diluted in SignalBoost™ Solution 2 (Merck), and enhanced Luminata Forte chemiluminescence reagent (Merck). Optical density of bands was quantified using densitometry (Quantity One) and normalised to a β-actin loading control.

Luciferase Reporter Assay

Hela cells were cultured in RPMI-1640 10% FCS. The day before transfection cells were detached with trypsin and seeded at $1.5x10^5$ cells per well in 6 well plates. 18 hours post seeding the media was changed to serum/antibiotic-free RPMI 1640 with L-Glutamine. 4 hours after the cells were transfected with Lipofectamine 2000 (Invitrogen) vector. A transfection mix containing Lipofectamine 2000 (1:500 ratio) in serum/antibiotic-free RPMI 1640 with L-Glutamine, 25ng Renilla and 500ng Eln luciferase reporter plasmid were added to all cells. Cells were co-incubated for 4 hours at 37°C, with

anti-has-miR-181b miScript miRNA inhibitor (10nM) or a miScript Inhibitor Negative Control (Qiagen; cat. No. 1027272) termed 'scrambled control', and then RPMI/FCS added to all relevant samples. 24 hours after transfection samples were collected in Dual-luciferase Assay Lysis buffer (Promega). Samples were prepared and quantified in accordance with the kit datasheet.

Study approval

Mice - The housing and care of the animals and all the procedures used in these studies were performed in accordance with the ethical guidelines and regulations of the University of Bristol and the UK Home Office. The investigation conforms to the Guide for the Care and Use of Laboratory Animals published by the US National Institutes of Health (NIH Publication No. 85–23, Eighth Edition, revised 2011). Adherence to the ARRIVE guidelines (10) for the reporting of animal in vivo experiments was also followed.

Human tissues – Coronary artery and aortic tissue segments were collected from cadaveric heart donors to the Bristol Coronary Artery Biobank under National Research Ethics Service approval (08/H0107/48). Written consent was obtained from the next of kin as part of the organ donation programme. Abdominal aortic aneurysm segments were collected from consenting patients undergoing aneurysm repair surgery under National Research Ethics Service approval (11/H0102/3). Consent was not required as the tissue is considered surplus.

Statistical Analysis

Values are expressed as mean ± standard error of the mean (SEM). Group values were compared using the computer program InStat (GraphPad). For the comparison of group means, a check was first made for normal distribution: if this was passed then an unpaired two sample two-tailed Student's t-test was carried out. If the variances were significantly different, then a Welch's correction test was used. Statistical differences between monocyte/macrophages from the same preparation were analysed by Students paired t-test. For the comparison of multiple groups, an analysis of variance (ANOVA) test was used, and a Student–Newman–Keuls multiple comparisons post hoc test employed when statistical differences were detected. Contingency data (for example aneurysm incidence) were analysed by Fisher's exact test. All in vivo and histological analyses were performed by two investigators in a blinded fashion. To demonstrate the robust assessment of semi-quantitative parameters such as plaque macrophage content and positivity for TIMP-3, intra- and inter-observer variability was determined by Bland –Altman plots. In all cases, statistical significance was concluded where the two-tailed probability was less than 0.05.

References

1. Singh RJR, Mason JC, Lidington EA, Edwards DR, Nuttall RK, Khokha R, Knauper V, Murphy G, Gavrilovic J. Cytokine stimulated vascular cell adhesion molecule-1 (VCAM-1) ectodomain release is regulated by TIMP-3. *Cardiovasc Res.* 2005;67:39-49.
2. Johnson JL, Fritsche-Danielson R, Behrendt M, Westin-Eriksson A, Wennbo H, Herslof M, Elebring M, George SJ, McPheat W, Jackson CL. Effect of Broad-Spectrum Matrix Metalloproteinase Inhibition on Atherosclerotic Plaque Stability. *Cardiovasc Res.* 2006;71:586-95.
3. Veniant MM, Withycombe S, Young SG. Lipoprotein size and atherosclerosis susceptibility in Apoe(-/-) and Ldlr(-/-) mice. *Arterioscler Thromb Vasc Biol.* 2001;21:1567-70.
4. Daugherty A, Manning MW, Cassis LA. Angiotensin II promotes atherosclerotic lesions and aneurysms in apolipoprotein E deficient mice. *J Clin Invest.* 2000;105:1605-12.
5. Daugherty A, Manning MW, Cassis LA. Antagonism of AT2 receptors augments Angiotensin II-induced abdominal aortic aneurysms and atherosclerosis. *Br J Pharmacol.* 2001;134:865-70.
6. Di Gregoli K, Jenkins N, Salter R, White S, Newby AC, Johnson JL. MicroRNA-24 Regulates Macrophage Behavior and Retards Atherosclerosis. *Arterioscler Thromb Vasc Biol.* 2014;34:1990-2000.

7. Quillard T, Tesmenitsky Y, Croce K, Travers R, Shvartz E, Koskinas KC, Sukhova GK, Aikawa E, Aikawa M, Libby P. Selective Inhibition of Matrix Metalloproteinase-13 Increases Collagen Content of Established Mouse Atherosclerosis. *Arterioscler Thromb Vasc Biol.* 2011;31:2464-72.
8. Shiomi M, Ito T, Hirouchi Y, Enomoto M. Fibromuscular cap composition is important for the stability of established atherosclerotic plaques in mature WHHL rabbits treated with statins. *Atherosclerosis.* 2001;157:75-84.
9. Kim SS, Ye CT, Kumar P, Chiu I, Subramanya S, Wu HQ, Shankar P, Manjunath N. Targeted Delivery of siRNA to Macrophages for Anti-inflammatory Treatment. *Mol Ther.* 2010;18:993-1001.
10. Kilkenny C, Browne WJ, Cuthill IC, Emerson M, Altman DG. Improving Bioscience Research Reporting: The ARRIVE Guidelines for Reporting Animal Research. *PLoS Biol.* 2010;8:e1000412.

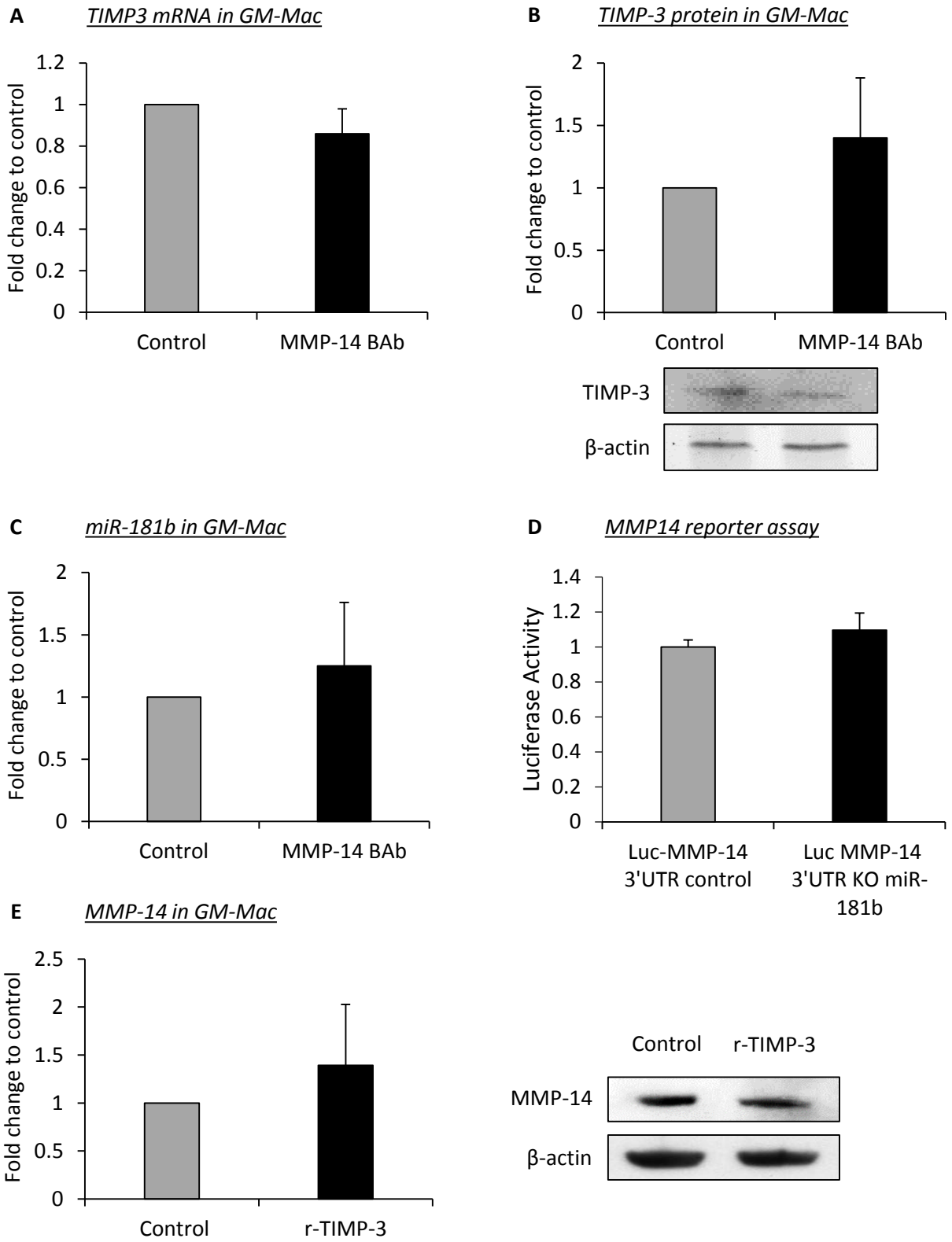

Supplemental Figure I: TIMP-3 and miR-181b expression are not regulated by MMP-14, and MMP-14 is not a miR-181b target gene

(**A**) QPCR and (**B**) western blot of TIMP-3 mRNA and protein expression respectively, in human macrophages differentiated in the presence of GM-CSF and treated with a MMP-14 blocking antibody (BAb; 15ng/ml) or mouse IgG to serve as a control, n=4/group. (**C**) QPCR of miR-181b in human macrophages differentiated in the presence of GM-CSF and treated with a MMP-14 blocking antibody (BAb; 15ng/ml) or mouse IgG to serve as a control, n=4/group. (**D**)) 3'-UTR luciferase reporter activity of human MMP14 in HeLa cells treated with a miR-181b inhibitor or a scrambled control, n=6. (**E**) Western blot of TIMP-3 protein expression in human macrophages differentiated in the presence of GM-CSF and treated with recombinant TIMP-3 (10nM), n=4/group.

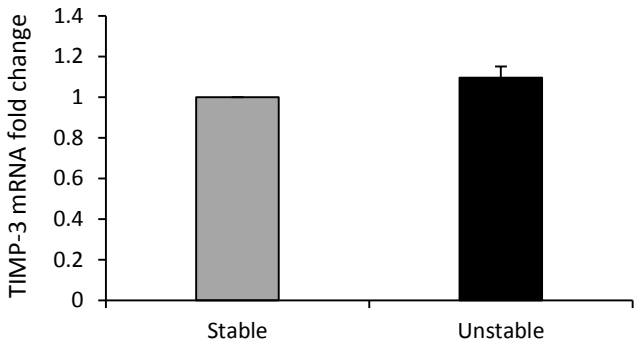

Supplemental Figure II: TIMP-3 mRNA expression is not altered between stable and unstable plaques

QPCR analysis of TIMP-3 mRNA expression from stable and unstable coronary atherosclerotic plaques, n=10/group. Data is expressed as fold change in expression compared to stable plaques, which is normalised to Scarna17 expression and set to 1.

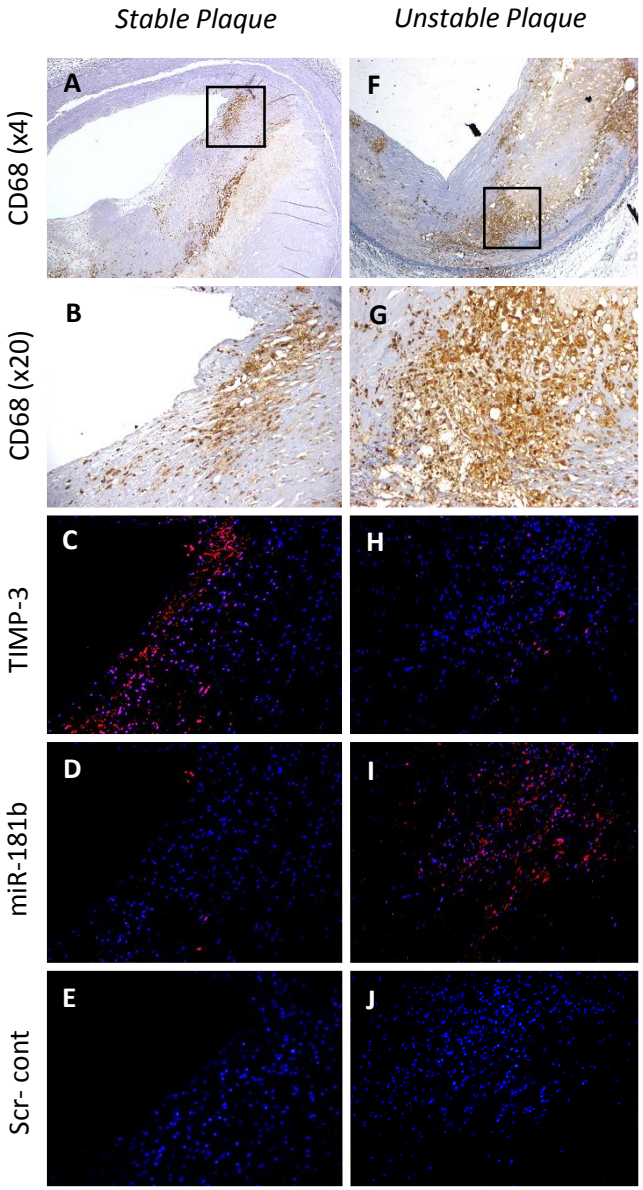

Supplemental Figure III: MicroRNA-181b expression is inversely related to macrophage TIMP-3 expression and plaque stability in human coronary atherosclerosis

Representative images of CD68 (for macrophages) and TIMP-3 protein expression by immunohistochemistry, and miR-181b or a scrambled LNA oligonucleotide to serve as a negative control (Scr-cont) by in situ hybridisation, from stable (A-E) and unstable (F-J) coronary atherosclerotic plaques, n=10/group. Box in A and F, higher magnification in B–E and G–J, respectively.

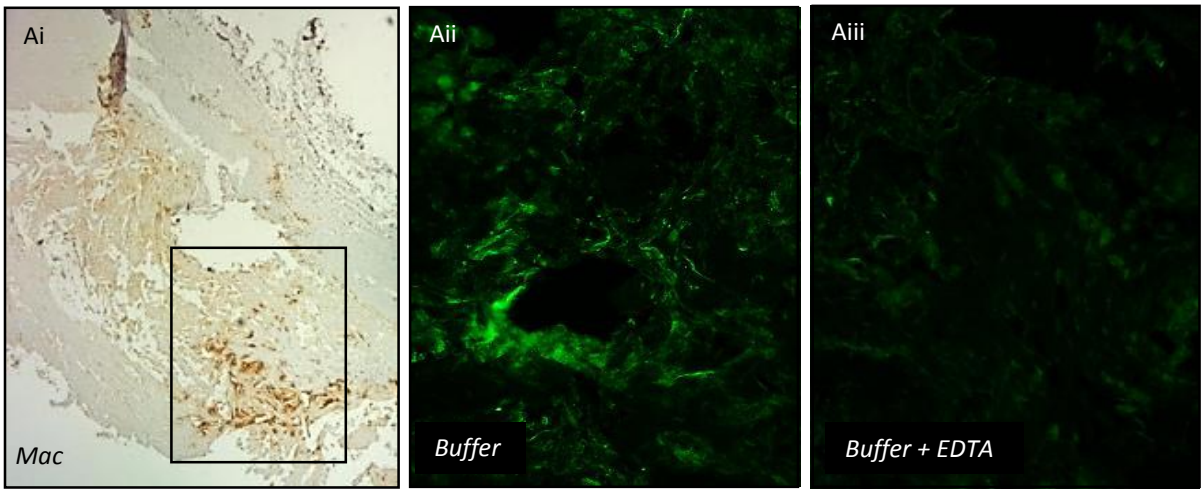

Supplemental Figure IV: Macrophage infiltration in human AAAs is associated with MMP activity
Human atherosclerotic abdominal aortic aneurysms demonstrating macrophage infiltration (Ai; macrophages labelled with CD68 – brown colour) which is associated with MMP activity as assessed by in situ zymography (green colour; Aii) as it can be retarded by a MMP inhibitor (EDTA; Aiii). Panels Aii, Aiii, are high power images from area indicated by black box in panel Ai.

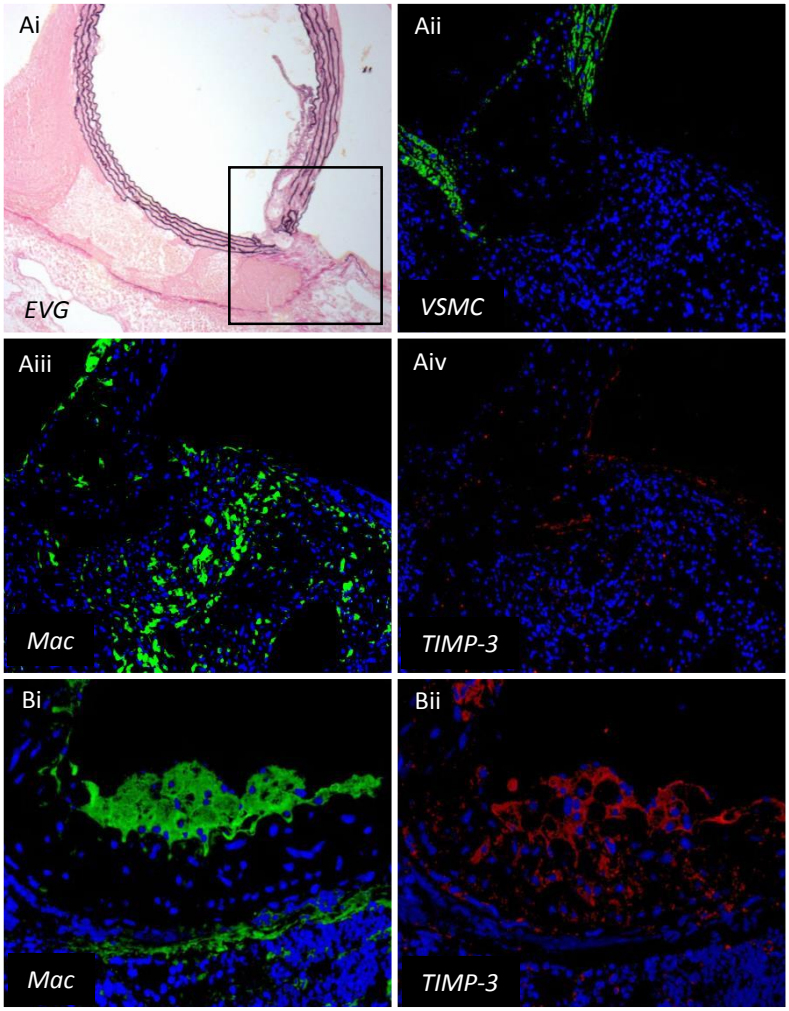

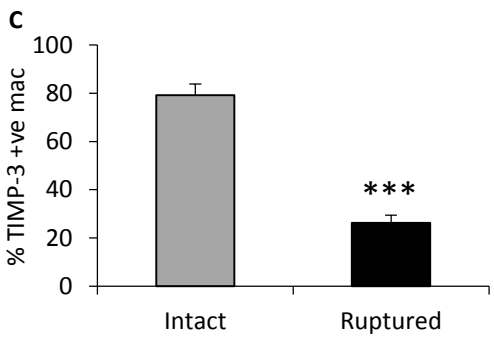

Supplemental Figure V: Diminished macrophage TIMP-3 expression associates with ruptured mouse aneurysms

(**A** and **B**) Analysis of atherosclerotic abdominal aortic aneurysms from Apoe$^{-/-}$ mice which have received Ang II and fed a high-fat diet for 4 weeks, and assessed by EVG for elastin breaks and atherosclerosis (Ai), α-smooth muscle actin for VSMC (green colour; Aii), F4/80 for macrophages (green colour; Aiii) and TIMP-3 (red colour; Aiv). Box in panel Ai represents high power field in panels Aii-Aiv. Non-aneurysmal arteries with abundant macrophages (green colour; Bi) and TIMP-3 (red colour; Bii). Nuclei are counterstained with DAPI (blue).

(**C**) Quantification of TIMP-3 positive macrophages (CD68) as assessed by immunofluorescence staining of ruptured and non-ruptured atherosclerotic AAAs from Ang II-infused 8 week high fat-fed Apoe$^{-/-}$ mice, n=6/group, ***P<0.000315, two-tailed Student's t-test, data expressed as mean±SEM.

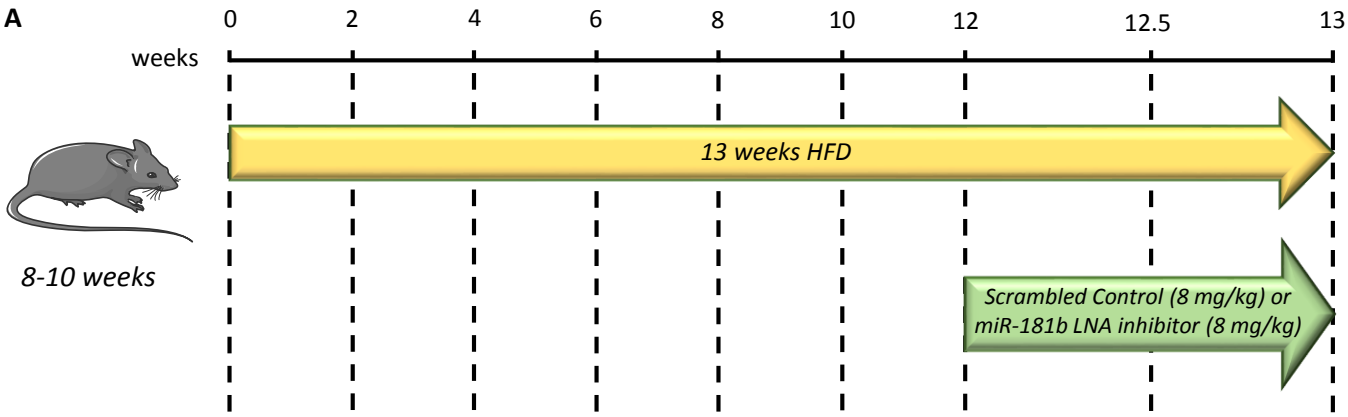

Supplemental Figure VI: Experimental design for atherosclerosis studies

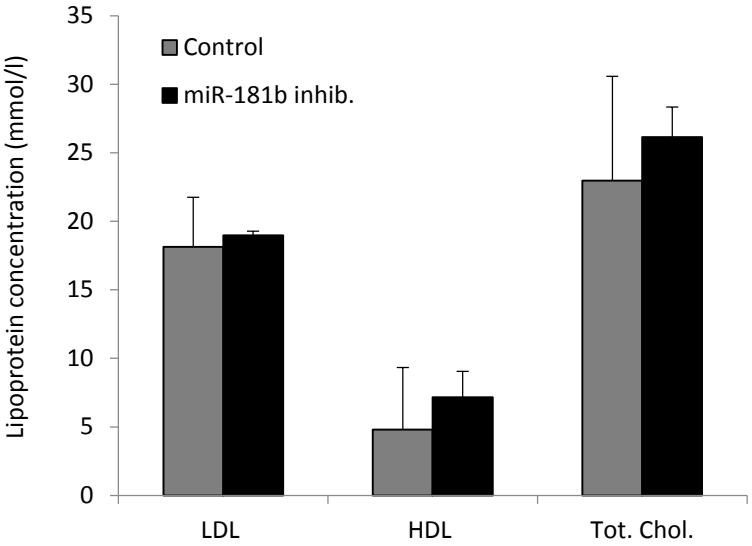

Supplemental Figure VII: Effect of miR-181b inhibition on plasma lipids in high-fat fed Apoe $^{-/-}$ mice
Quantification of plasma lipid profiles performed on terminal bloods drawn from the abdominal aorta of 13 week high-fat fed Apoe $^{-/-}$ mice after 1 week treatment of miR-181b inhibitor or a scrambled control, n=6/group, data expressed as mean±SEM.

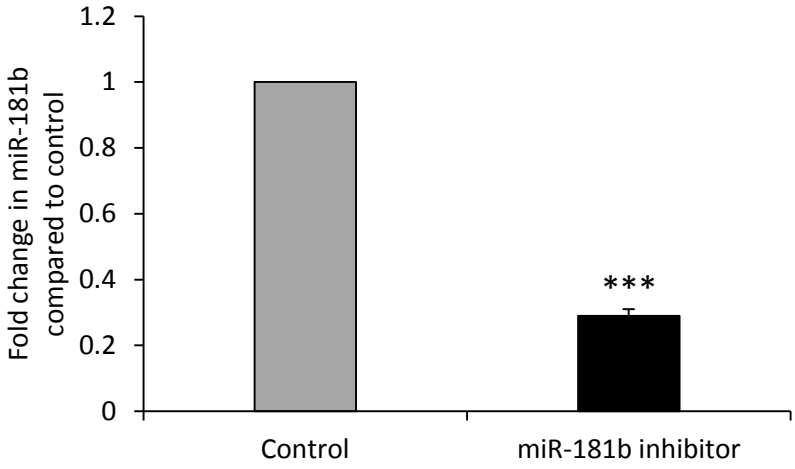

Supplemental Figure VIII: Effect of miR-181b inhibition on intra-plaque miR-181b expression
QPCR analysis and quantification of miR-181b expression in atherosclerotic brachiocephalic arteries from scr-control & LNA-miR-181b inhibitor treated mice, demonstrating that miR-181b expression was significantly reduced through miR-181b inhibition (n=6/group; ***p=0.000425 compared to scrambled control mice, two-tailed Student's *t*-test). Data is expressed as fold change in miR-181bexpression compared to controls, which is normalised to Scarna17 expression and set to 1.

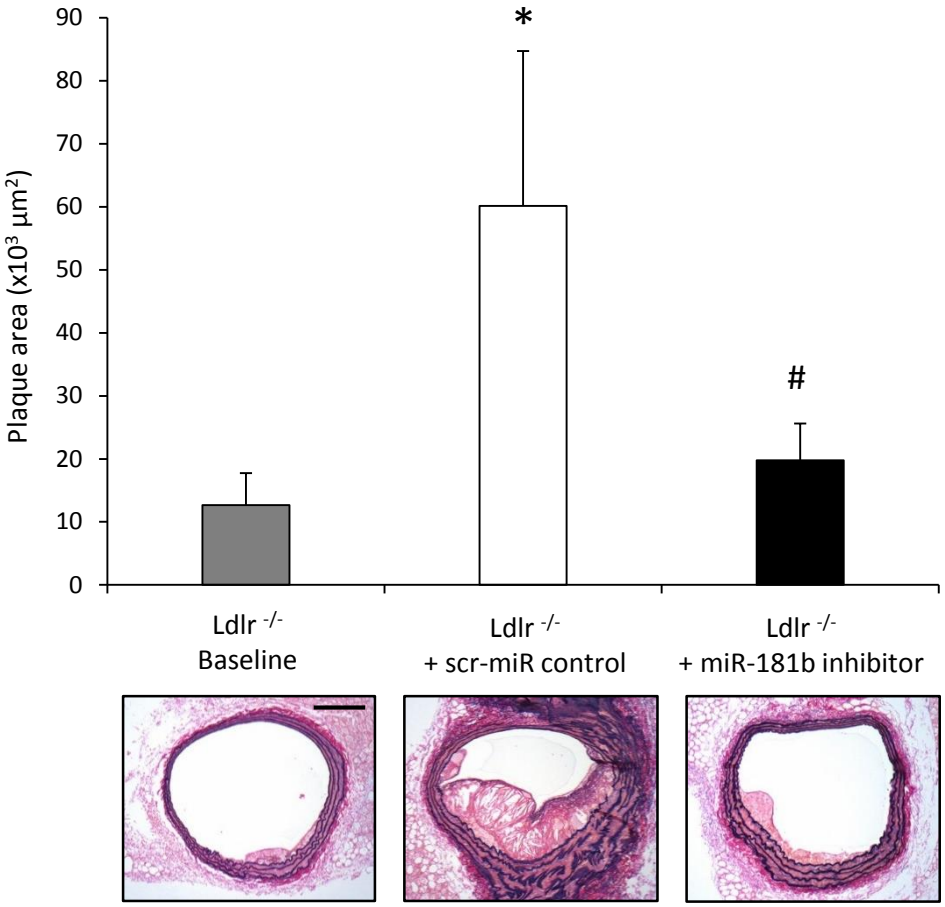

Supplemental Figure IX: miR-181b inhibition stabilises atherosclerotic plaques in hypercholesteroleamic Ldlr $^{-/-}$ mice

Representative images and quantification of plaque cross-sectional area in EVG-stained sections of plaques within the brachiocephalic artery, of Ldlr $^{-/-}$ mice high fat-fed for 8 weeks (baseline), or 12 weeks and scrambled (scr) control or miR-181b inhibitor-treated between 8 and 12 weeks of high fat-feeding, n=6-8/group, *P<0.05 compared to Ldlr $^{-/-}$ baseline mice, $^{\#}P$<0.05 compared to Ldlr $^{-/-}$ scrambled control animals, ANOVA, scale bar represents 100µm and is applicable to all panels. Data represents the mean±SEM.

A. *Progression*

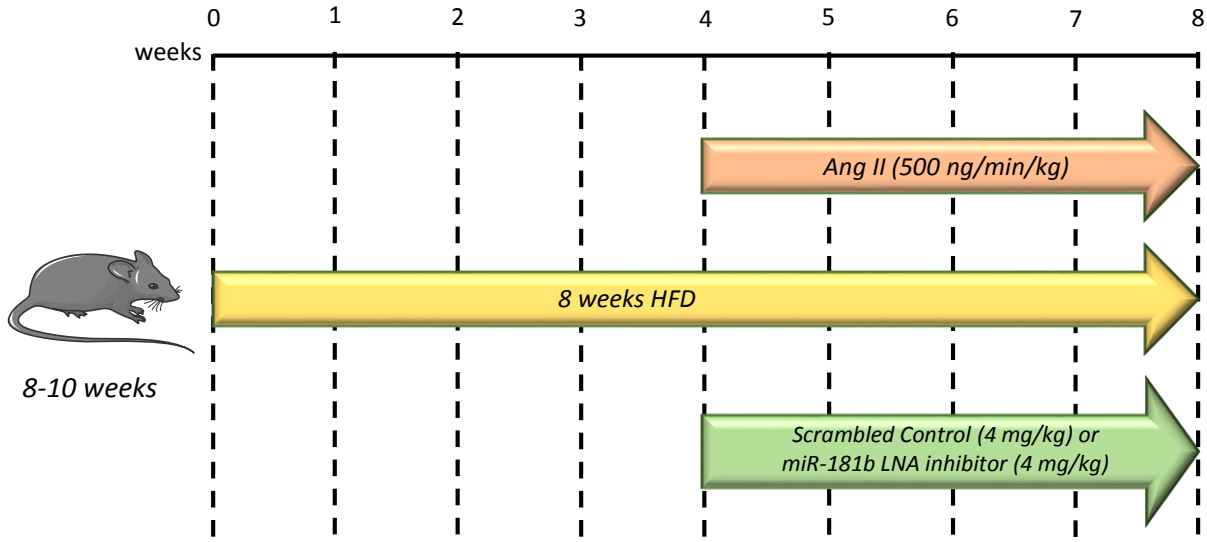

B. *Regression*

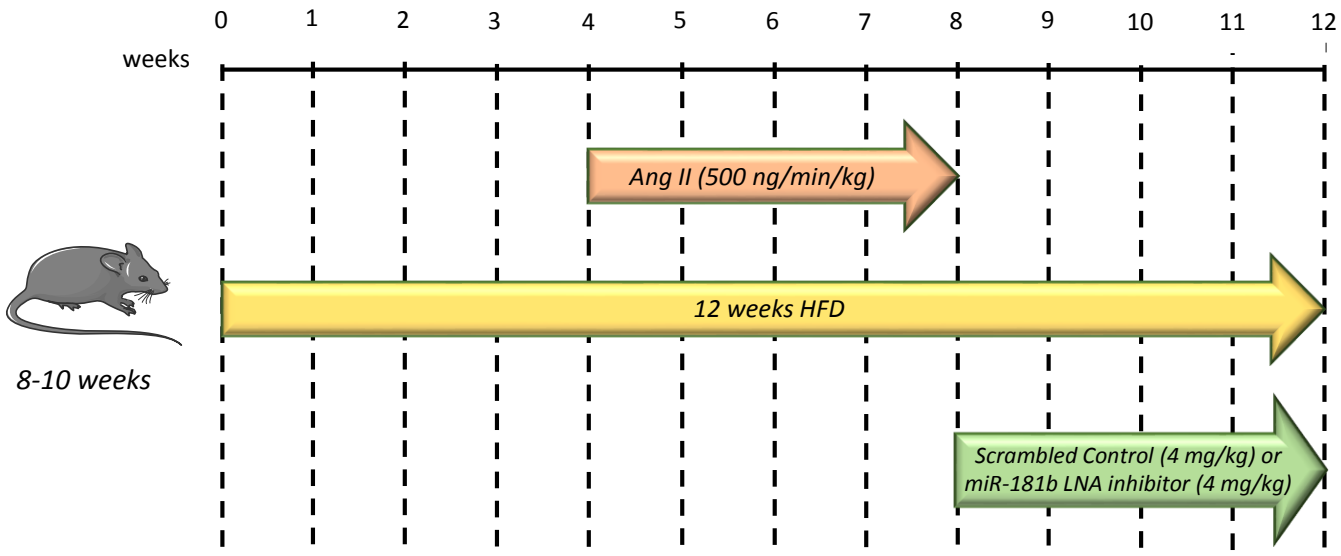

Supplemental Figure X: Experimental design for aneurysm studies

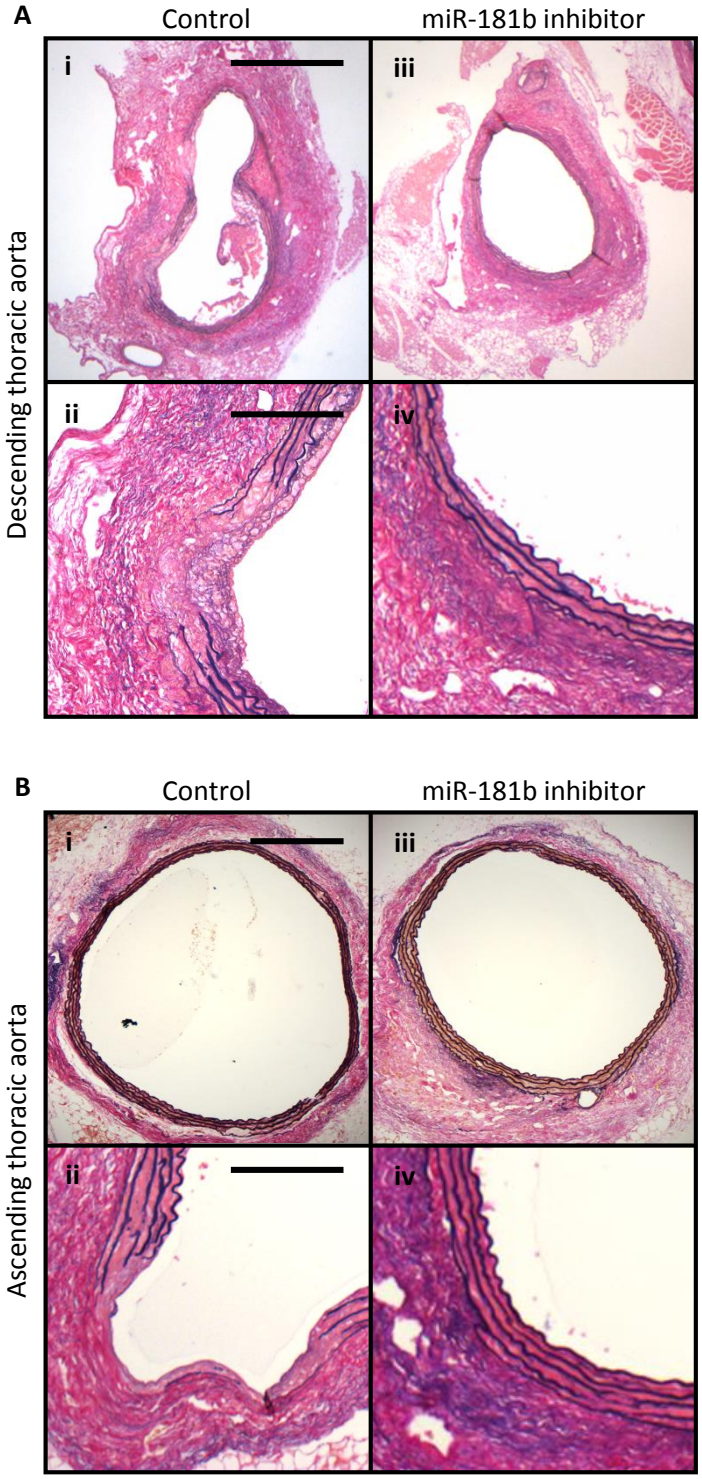

Supplemental Figure XI: miR-181b inhibition regulates elastin content and fragmentation at multiple aneurysmal sites in *Ldlr* $^{-/-}$ mice

Representative images of elastin van Gieson stained histological cross-sections of (**A**) descending and (**B**) ascending thoracic aortae from scrambled control and miR-181b inhibitor-treated *Ldlr* $^{-/-}$ mice, demonstrating differences in elastin (black) content and fragmentation, scale bar in Ai represents 200µm and is applicable to Ai and Aiii, scale bar in Aii represents 50µm and is applicable to Aii and Aiv, scale bar in Bi represents 100µm and is applicable to Bi and Biii, scale bar in Bii represents 50µm and is applicable to Bii and Biv.

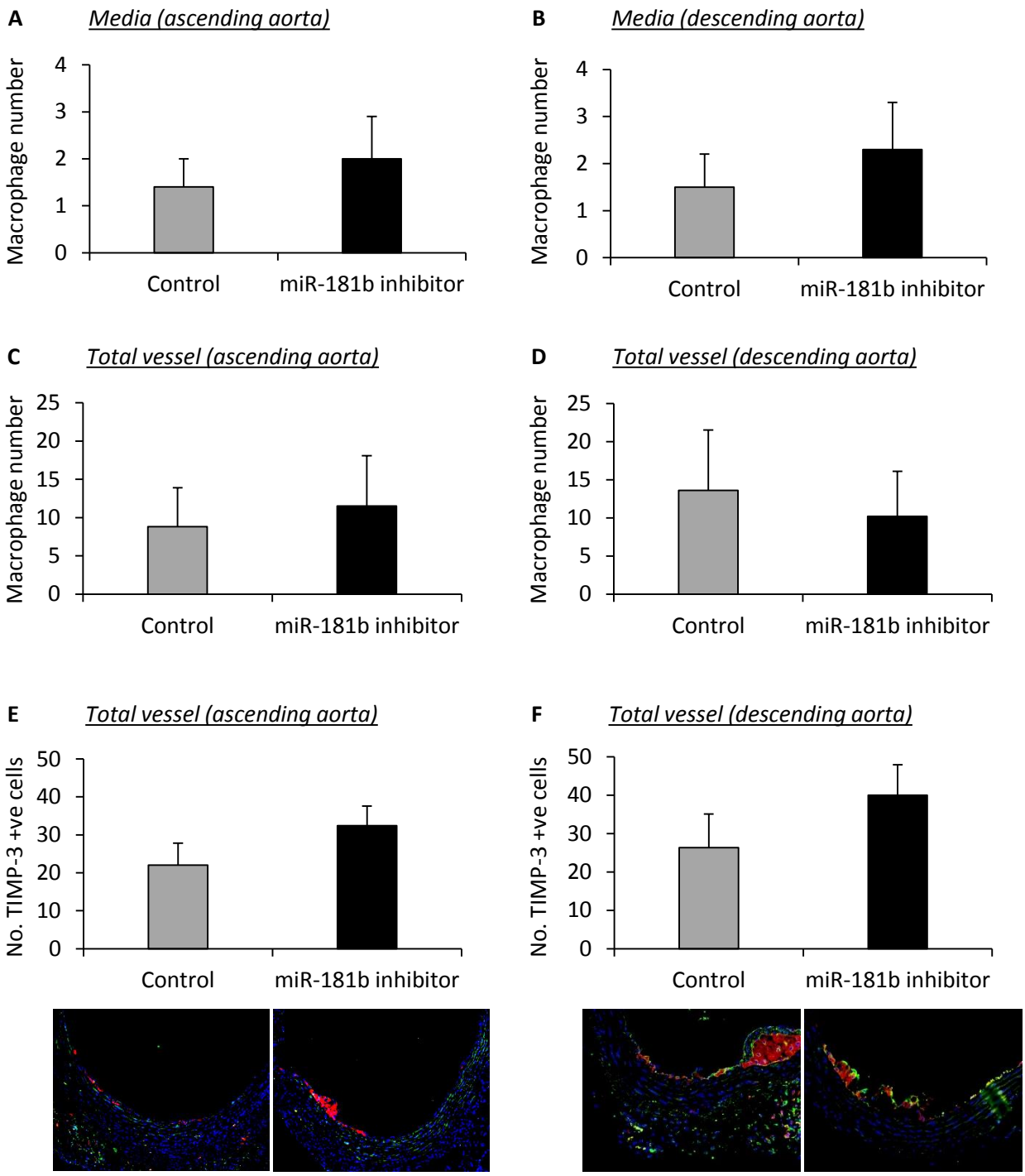

Supplemental Figure XII: Effect of miR-181b inhibition on macrophage content and TIMP-3 expression in ascending and descending aortas from *Apoe* $^{-/-}$ mice

Quantification and representative images of CD68 and TIMP-3 immuno-histochemical labelled cross-sections of (**A, C and E**) ascending and (**B, D and F**) descending thoracic aortae from scrambled control and miR-181b inhibitor-treated *Apoe* $^{-/-}$ mice. In representative images, red depicts CD68 (macrophages), green depicts TIMP-3, and blue indicates nuclei (Dapi).

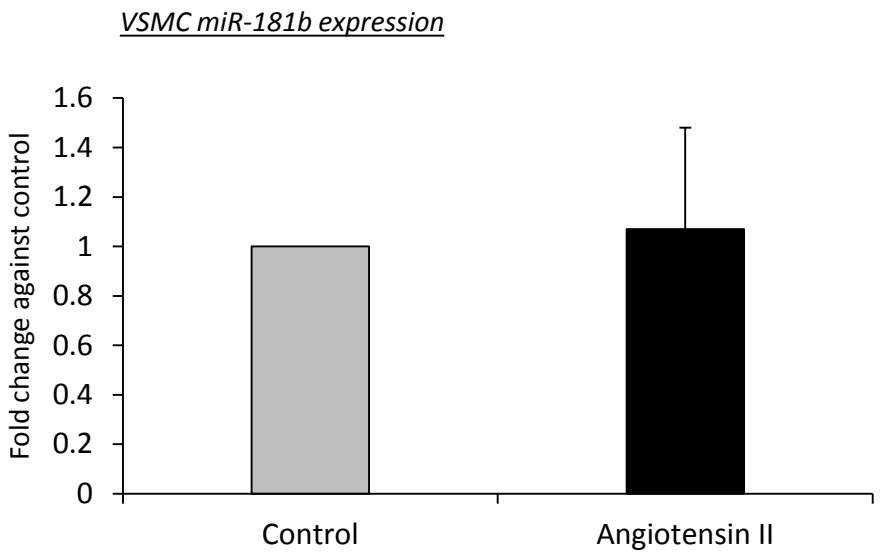

Supplemental Figure XIII: Angiotensin II does not regulate VSMC miR-181b expression
QPCR for miR-181b expression in VSMCs after 6 hour stimulation with angiotensin II (5μM) or PBS to serve as a control (n=4).

A *Intraobserver agreement*

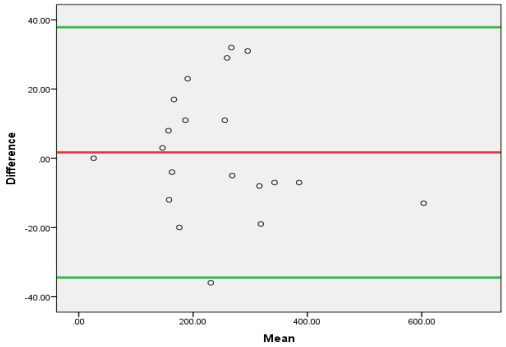

Coefficients[a]

Model		Unstandardized Coefficients		Standardized Coefficients		
		B	Std. Error	Beta	t	Sig.
1	(Constant)	7.720	9.804		0.787	0.441
	Mean	-0.025	0.036	-0.158	-0.679	0.506

a. Dependent Variable: Difference

B *Interobserver agreement*

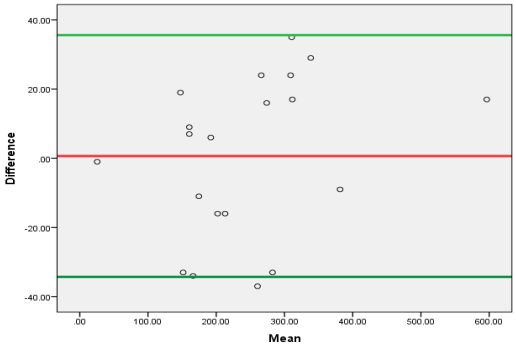

Coefficients[a]

Model		Unstandardized Coefficients		Standardized Coefficients		
		B	Std. Error	Beta	t	Sig.
1	(Constant)	-14.259	11.831		-1.205	0.244
	Mean	0.061	0.044	0.312	1.391	0.181

a. Dependent Variable: Difference

Supplemental Figure XIV: Assessment of intra- and inter-observer variability in histological assessment of intra-plaque TIMP-3 positive macrophages

Bland-Altman plots and associated statistical evaluation demonstrating good intra-observer (A) and inter-observer (B) agreement of TIMP-3 positive macrophages in stable and unstable human coronary artery atherosclerotic plaques. The red line indicate the mean, whilst the green lines depict upper and lower confidence levels.

Supplemental Table I: List of primary antibodies

Antibody	Application	Dilution	Company	Code
Alpha-Smooth Muscle Actin	IHC	1/400	Sigma	A2547
β-Actin	WB	1/10000	Sigma	A5316
Cleaved Caspase 3	IHC	1/100	Cell Signalling	#9664
CD68	IHC (Ms)	1/100	Santa Cruz	sc-7084
CD68	IHC (Hm)	1/100	Dako	M0814
Elastin	WB	1/200	Santa Cruz	sc-17580
GSLII	IHC	1/200	Vector Labs	B-1215
GM-CSF	IHC	1/50	R&D Systems	MAB215
PCNA	IHC	1/100	Cell Signalling	#13110
TIMP-3	IHC	1/200	Millipore	MAB3318
TIMP-3	IHC / WB	1/200 / 1/1000	Abcam	ab39184

Supplemental Table II: List of Q-PCR primers

Gene/Primer ID	Species		Sequence
Acta2	Ms	Forward	TTCGTGACTACTGCCGAGCGTG
		Reverse	GAGAGTCTCTGGGCAGCGGAAG
ActB	Ms	Forward	AGGCGGACTGTTACTGAGCTGC
		Reverse	CTGTCGCCTTCACCGTTCCAGT
Bax	Ms	Forward	CTGGATCCAAGACCAGGGTG
		Reverse	CCTTTCCCCTTCCCCCATTC
Cd68	Ms	Forward	TGGCGGTGGAATACAATGTGTC
		Reverse	GACTGGTCACGGTTGCAAGAGA
p53	Ms	Forward	AGGATGCCCATGCTACAGAG
		Reverse	TGAGTGGATCCTGGGGATTGTG
TIMP3	Hm	Forward	CTTCCGAGAGTCTCTGTGGCCTTA
		Reverse	CTCGTTCTTGGAAGTCACAAAGCA
Timp3	Ms	Forward	CACATCAAGGTGCCATTCAGGTAG
		Reverse	GTTCTCTCCTCCTCAACCCAAACA